

Design and Analysis of Marine Propeller

By

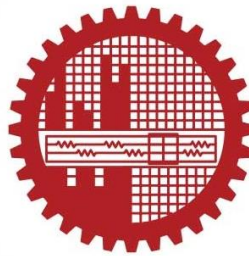
Md. Asaduzzaman (Student ID:201612014)

Md. Imdadul Haque (Student ID:201612016)

Md. Zahidul Islam Laku (Student ID:201612020)

A thesis submitted to the
Department of Naval Architecture and Marine Engineering
in partial fulfillment of the requirements for the degree of
Bachelor of Science
in
Naval Architecture and Marine Engineering.

Supervisor: Dr. Md. Shahjada Tarafder
Professor, Department of NAME (BUET)



Bangladesh University of Engineering and Technology (BUET)

Dhaka-1000, Bangladesh.

May 2022

Contents

ACKNOWLEDGEMENT	4
ABSTRACT	5
1. INTRODUCTION	6
1.1 Literature Review.....	6
1.2 Objectives Of Present Research.....	8
2 THEORETICAL FRAMEWORK	9
2.1 Open Water Characteristics	9
2.2 Standard Series Data	10
2.3 Governing Equations	14
3 DESIGN AND ANALYSIS	16
3.1 Definition of the Problem	16
3.2 Design	17
3.3 Geometry Generation.....	22
3.4 Analysis.....	23
3.4.1 Domain.....	24
3.4.2 Boolean	24
3.4.3 Meshing.....	25
3.4.4 Setup & Simulation.....	29
4 RESULTS AND DISCUSSIONS	36
4.1 Conventional Propeller	36
4.2 Ducted Propeller	39
5 CONCLUSIONS	41
6 REFERENCES	42
APPENDIX	45
Appendix A: Resistance calculation by Holtrop and Mennen method	45
Appendix B: Taylor wake fraction.....	48
Appendix C: Thrust, Torque and Delivered power calculations.....	49
Appendix D: Propeller geometry	50
Appendix E: Duct geometry	52
Appendix F: Step by step Ansys setup for simulation	53

List of Tables

<i>Table 2.1: Coefficients for the polynomials form of K_T and K_Q</i>	12
<i>Table 3.1: Problem Specification</i>	16
<i>Table 3.2: Design Constraints</i>	17
<i>Table 3.3: K_Q for different J values for fixed PD</i>	18
<i>Table 3.4: K_Q for different pitch ratio</i>	19
<i>Table 3.5: Intersection data points</i>	20
<i>Table 3.6: Optimum Values</i>	21
<i>Table 3.7: Open water data for optimum pitch ratio</i>	21
<i>Table 3.8: Details of meshing</i>	25
<i>Table 3.9: Details of Sizing</i>	26
<i>Table 3.10: Details of Method</i>	26
<i>Table 3.11: Mesh sensitivity analysis</i>	28
<i>Table 4.1: Open water data using regression analysis</i>	36
<i>Table 4.2: Open water data of numerical analysis using ANSYS</i>	37
<i>Table 4.3: Percentage difference between Theoretical and Numerical Analysis</i>	38
<i>Table 4.4: Error percentage for optimum value</i>	38
<i>Table 4.5: Comparison with the mentioned paper</i>	39
<i>Table 4.6: Open water data of the ducted propeller</i>	39

List of Figures

Figure 3.1: Open water diagram for pitch ratio 1.0	18
Figure 3.2: KQ over advance coefficient for given PD	19
Figure 3.3: KQ Intersection for different pitch ratio	20
Figure 3.4: Maximum open water efficiency	20
Figure 3.5: Open water diagram for optimum pitch ratio	22
Figure 3.6: Geometry of the propeller in PropCad	22
Figure 3.7: 3D model of the propeller in Rhinoceros	23
Figure 3.8: Ducted propeller model in Rhinoceros	23
Figure 3.9: Scheme of the propeller and fluid domain	24
Figure 3.10: Meshing of Static and Rotary Domain (Conventional)	27
Figure 3.11: Meshing of the propeller(conventional)	27
Figure 3.12: Mesh convergence	28
Figure 3.13: Meshing of Static and Rotary Domain (Ducted)	29
Figure 3.14: Meshing of propeller and duct	29
Figure 3.15: Residuals (conventional, $J=0.6$)	30
Figure 3.16: Thrust force (conventional, $J=0.6$)	31
Figure 3.17: Pressure contour (conventional, $J=0.6$)	31
Figure 3.18: Velocity contour (conventional, $J=0.6$)	31
Figure 3.19: Velocity streamlines (conventional, $J=0.6$)	32
Figure 3.20: Turbulence kinetic energy (conventional, $J=0.6$)	32
Figure 3.21: Residuals (ducted, $J=0.5$)	32
Figure 3.22: Thrust force (ducted, $J=0.5$)	33
Figure 3.23: Pressure contour (ducted, $J=0.5$)	33
Figure 3.24: Velocity contour (ducted, $J=0.5$)	34
Figure 3.25: Turbulence kinetic energy (ducted, $J=0.5$)	35
Figure 3.26: Velocity streamlines (ducted, $J=0.5$)	35
Figure 4.1: Open water diagram of conventional propeller using regression analysis	36
Figure 4.2: Open water diagram of numerical analysis	37
Figure 4.3: Open water diagram comparing Numerical Analysis with the Theoretical Value	38
Figure 4.4: Open water diagram	40
Figure 4.5: Comparison between conventional and ducted propeller	40

ACKNOWLEDGEMENT

Dr. Md. Shahjada Tarafder, Professor of the Department of Naval Architecture and Marine Engineering at Bangladesh University of Engineering and Technology (BUET), Dhaka-1000, Bangladesh, is owed a great debt of gratitude for his helpful suggestions and cooperation throughout the course of this research project. Without his counsel and assistance, this initiative would not have been a success. The completion of this research was made possible by his constant supervision, constructive criticism, valuable advice, scholarly guidance, and momentary encouragement, as well as his wholehearted support by providing all papers, books, and internet materials related to this research and other facilities. We are quite grateful to the seniors who assisted us with the procedures. The department of Naval Architecture and Marine Engineering at Bangladesh University of Engineering and Technology (BUET), Dhaka-1000, Bangladesh, receives our best wishes.

We are most grateful to Allah Almighty for the successful completion of the project.

ABSTRACT

This thesis investigates the design and analysis of a marine propeller. Here both conventional and ducted propeller will be investigated. Wageningen-B series propeller is chosen. The complete 3D geometry generation of this propeller includes the use of the software PropCad and Rhinoceros. The geometry is numerically analyzed by solving Reynolds Average Navier Stokes (RANS) equation. Multiple RANS solver can be used for Computational Fluid Dynamics (CFD) simulation. $k-\epsilon$ turbulence model is used for its better performance on propeller analysis where the discretization is done by Finite Volume Method (FVM). The numerical result is then compared with the results obtained from well-established polynomial formulae for Wageningen-B series propeller. The same propeller is numerically analyzed again after fitted with a 19A duct on it. It is important to have as little space as possible between the tip of the blades and the duct to achieve optimal performance. The clearance in this instance is 15 millimeters, which is less than one percent of the diameter of the propeller. This enables a comparison of the performance of ducted propellers and conventional propellers across a range of speeds while adhering to the same set of restrictions.

Grid independence test is essential for providing a more accurate estimation of the results within a particular time frame. Mesh sensitivity analysis is carried out based on thrust and torque coefficients.

1. INTRODUCTION

The present maritime industry is substantially more competitive than it was in previous decades. So, to achieve high speed and low power consumption, ongoing research and enhancement of marine propellers is carried out.

At first, the ideal way for testing propeller performance is to use a steady flow. Then performance may be measured for non-uniform flow, which is more representative of real-world propeller performance. The measurement of cavitation is a crucial aspect in the process of determining propeller performance. Cavitation reduces propeller performance. Hence accurate cavitation estimation is required for effective propeller design. Moreover, the geometry of propeller is complex one. These factors, together with additional limitations, make accurate CFD simulation of propeller flow one of the difficult one for researchers as well as for designers.

In the past, propeller design used to be entirely based on design charts that were created by fitting theoretical models to data obtained from actual models. For instance, the Wageningen B-series has been numerically adapted into polynomial regression, making interpolation and optimization with traditional blade geometries simple. This approach is still common at the outset of a propeller design. However, to design an efficient and optimized propeller within given constraints, nowadays, computer tools and techniques have been introduced.

1.1 Literature Review

CFD techniques have shown great promise in terms of designing a propeller that is both efficient and optimized. CFD simulations are now being used by a growing number of researchers. Some of them achieve better results than the traditional propeller design method.

[Funeno \(2002\)](#) simulated the current around a highly skewed propeller via unstructured mesh. For steady state and unsteady flow, he obtained good correspondence with experimental data, but this method was complicated and time consuming. [Martínez-Calle et al. \(2002\)](#) simulated the propeller via $k - \epsilon$ turbulence method in open water in steady state condition. The results were acceptable but there was approximately 30% error in prediction of the torque coefficients. [Watanabe et al. \(2003\)](#) simulated the propeller via standard $k - \omega$ turbulence method in open water and steady state conditions. He used the propeller symmetry and simulated only one blade, comparing to the experimental tests, he got 15 percent of error. [TREJO et al. \(2007\)](#) performed numerical analysis of a marine propeller using ANSYS CFX 11. They simulated first with full model and then taking only one blade. They obtained less than 10% error in thrust and torque coefficients comparing to experimental results. [Mossad et al. \(2011\)](#) provided a complete guideline for geometry generation, boundary conditions, setup, simulation, problems to achieve accurate results using CFD for marine propeller analysis. They used both $k - \epsilon$ and $k - \omega$ turbulence model and showed better agreement with the experimental results. They concluded that $k - \epsilon$ has over-predicted. Hence, $k - \omega$ is suitable. [Prakash and Nath \(2012\)](#) investigated four bladed Wageningen B screw series propeller and numerically analyzed using unstructured mesh. [Parra \(2013\)](#) performed CFD simulation and use lifting line theory for

propeller analysis. But found no correlation in the differences between RANS analysis and the lifting line theory. But obtain good result even for higher high advance ratio (up to $J=1$). [Elghorab et al. \(2013\)](#) performed numerical simulation of a marine propeller using ANSYS CFX and compared with the experimental results. They obtained 10.59% of error in thrust coefficient and 18.9% of error in torque coefficient. They obtained suitable mesh model through grid convergence test. Through extension in CFD simulation, they have proved that the model provides good agreement with the B-series curves. [Kolakoti et al. \(2013\)](#) performed CFD analysis of bare hull of a ship, open water analysis of a controllable pitch propeller and flow characteristics of that propeller attached with the same hull. They compared the numerical results with the experimental results and obtained 4% and 14% error in thrust and torque in operational regime of the propeller. They have observed here and that is the propeller-hull interaction. [Turunen et al. \(2014\)](#) analyzed a marine propeller using the method available in openFOAM and found that the simpleFoam code predicts forces well in the case of a single propeller with multiple reference frame (MRF). [Harish et al. \(2015\)](#) performed static analysis of a 4-bladed B-series marine propeller. They used PROPCAD and CATIA V5R20 for design purpose and ANSYS FLUENT for simulation. Analysis was done for different materials (aluminum, R glass, S2 glass, carbon epoxy) and showed that aluminum propeller provides minimum deformation. [DurgaNeeharika and Babu \(2015\)](#) developed the solid model of propeller in CATIA-V5 R20 and static analysis was carried out using ANSYS. They found that metallic propellers can be replaced by composite propellers for enhanced performance with regard to the operating range. [Saha et al. \(2018\)](#) performed CFD simulation of a Wageningen B-series propeller and compared with the results obtained from the empirical formula. The obtained lowest percentage of error in K_T and K_Q was 13%. [Triet et al. \(2018\)](#) performed CFD simulation for the Wageningen B-Series propeller and found $k - \epsilon$ turbulence model gives quite good result except at the high advance ratio ($J = 0.7$ and 0.75). The differences between simulation results and experimental data are lower than 10%. Mesh sensitivity analysis was carried out based on Y^+ value. [Bahatmaka et al. \(2018\)](#) investigated KP505 propeller where propeller problem was solved by OpenFoam and $k - \omega$ SST model was used for simulation. They obtained the best mesh configuration through grid convergence test. They compared the numerical results with the experimental results and obtained less than 2% error in thrust. [Boumediene et al. \(2019\)](#) studied the flow around Seiun Maru highly skewed marine propeller in both steady and unsteady case using Ansys Fluent and compared the performances with the experimental results. In steady case they obtained average error percentage of 4.18% and 6.04% in thrust and torque coefficients. From the unsteady case they concluded to bring the inlet boundary closer to the propeller. [Fitriadhy et al. \(2020\)](#) performed CFD analysis for different number of blades and found that three blade propellers are most efficient within the advance coefficient range between 0.8 to 0.9.

[Shreyash et al. \(2020\)](#) analyzed the propeller which is based on the coordinates of model KCD 32 (Emerson and Sinclair, 1967) and used SOLIDWORKS to recreate the geometry of a 3D geometry. The analysis was completed using a computational program, Ansys FLUENT. They found that low weight blade can be designed and manufactured with strong load carrying capacity and increase in efficiency of marine propeller on replacement with composite material by reducing its weight without compromising its strength.

Gaggero et al. (2012) designed ducted propeller using hybrid approach and numerically analyzed using RANS solver. They used decelerating type of duct and found reduce cavitation phenomenon. Yu et al. (2013) investigated Ka-Series propeller with a 19A duct by employing panel method and RANS code. They showed that the panel method shows reasonable accuracy in predicting the performance, but RANS method gives better result than panel method. Szafran et al. (2014) investigated the effects of duct shape on ducted propeller thrust performance and compared propulsion characteristics of the duct propeller with the conventional nozzle 19A and perspective nozzles NACA-73_4212 and Wartsila-HR in hovercraft operation conditions. Razaghian and Ghassemi (2016) investigated a 5-bladed B-series propeller using RANS code and compared and validated with the experimental results. They conducted mesh sensitivity analysis for thrust. Then they analyzed the same propeller with both accelerating (19A) and decelerating (N32) duct. They obtained that the 19A ducted propeller improved propeller characteristics while N32 model had a negative effect and at higher advance ratio the N32 ducted propeller is suitable and can increase thrust upto 13%. Majdfar et al. (2017) investigated the effect of length and angle of 19A type of duct on the hydrodynamic performance using SST $k - \omega$ turbulence model. Error percentage between numerical and experimental results was reasonable. They concluded that increase in duct length doesn't significantly change the thrust coefficient. Motallebi-Nejad et al. (2017) predicted the hydrodynamic forces acting on a pumpjet propulsion system. For that purpose, they first applied the SST $k - \omega$ turbulence model to a ducted propeller which was then applied to the pumpjet. They obtained fine grid solution with numerical uncertainty of 0.06% for the thrust coefficient and obtained good compatibility between the numerical and experimental results. Du and Kinnas (2019) designed and analyzed a Ka4-70 propeller with a 19A duct. They designed the ducted propeller by coupling a RANS/VLM (Vortex Lattice Method) with a nonlinear optimization method. They achieved the target thrust with a higher efficiency after a few iterations.

1.2 Objectives Of Present Research

The researcher mentioned above focuses on the simulation of fluid flow around the propeller as well as the propeller's efficiency. They use a variety of software and mathematical modeling techniques to achieve the goal. These studies have a significant impact on determining the optimal propeller and boosting propeller efficiency within certain restrictions. They employ traditional propellers with three blades, albeit some of them have different propeller blade numbers. They rarely compared the efficiency of ducted propeller with conventional propeller under the same set of constraints. In some circumstances, they employ series data to generate open water characteristics.

Objectives of this thesis are-

- To calculate open water characteristics of marine propeller using series data
- To generate the open water characteristics chart using Regression analysis
- To obtain the open water characteristics by simulating the design using Fluent
- To compare these two results

2 THEORETICAL FRAMEWORK

Traditional propeller design is experiment based. Based on the previous standard data an optimum geometry is obtained. Propeller open water characteristics and standard series data are used in this process. This geometry is then made ready for fluid flow simulation. Theories behind these are discussed in this chapter.

2.1 Open Water Characteristics

Even though the propeller operates in a very non-uniform ship wake, a standard propeller test is performed in uniform flow, yielding the so-called open-water characteristics. The open water characteristics of a propeller are terms that describe the forces and moments acting on the propeller while it is working in a uniform fluid stream. Thrust and torque coefficient of a propeller are important non-dimensional open water characteristics that help to estimate thrust and torque of a propeller.

Thrust coefficient:

$$K_T = \frac{T}{\rho \cdot n^2 \cdot D^4} \quad 2.1$$

Torque coefficient:

$$K_Q = \frac{Q}{\rho \cdot n^2 \cdot D^5} \quad 2.2$$

The advance coefficient J is defined by the following equation:

$$J = \frac{V_A}{n \cdot D} \quad 2.3$$

Using the formula of the advance coefficient J and replacing D in Eq.2.2 gives the following equation.

$$\frac{K_Q}{J^5} = \frac{P_D \cdot n^2}{2\pi \cdot \rho \cdot V_A^5} \quad 2.4$$

Using the equation above, a plot of K_Q over J can be easily obtained.

Velocity of advance is defined as follows.

$$V_A = V_S \cdot (1 - w) \quad 2.5$$

Where,

V_A is the velocity of advance

V_S is the speed of the ship

And, w is the wake fraction.

Propeller open water efficiency η_0 is derived in terms of thrust and torque coefficient and advance coefficient J . Using the Eq.2.1 and Eq.2.2 open water efficiency η_0 can be written as follows.

$$\eta_0 = \frac{T \cdot V_A}{2\pi \cdot n \cdot Q} = \frac{K_T \cdot \rho \cdot n^2 \cdot D^4}{K_Q \cdot \rho \cdot n^2 \cdot D^5} \cdot \frac{V_A}{2\pi \cdot n} = \frac{J}{2\pi} \cdot \frac{K_T}{K_Q} \quad 2.6$$

2.2 Standard Series Data

There are different types of blade geometries. Among them Wageningen-B series is the most common. The open water characteristics of Wageningen-B series are represented at a Reynolds Number 2×10^6 by the polynomials in the following form. (Barnitsas et al. 1981)

$$K_Q = \sum_{n=0}^{47} C_n(J)^{S_n} \left(\frac{P}{D}\right)^{t_n} \left(\frac{A_E}{A_0}\right)^{u_n} (Z)^{v_n} \quad 2.7$$

$$K_T = \sum_{n=0}^{39} C_n(J)^{S_n} \left(\frac{P}{D}\right)^{t_n} \left(\frac{A_E}{A_0}\right)^{u_n} (Z)^{v_n} \quad 2.8$$

The coefficients of the polynomials C, s, t, u, v can be found in the **Table 2.1**: Coefficients for the polynomials form of K_T and K_Q **Table 2.1**.

Table of Coefficients for the polynomials form of K_T and K_Q for $R_N=2 \times 10^6$											
Coefficients for K_T - polynomial						Coefficients for K_Q - polynomial					
n	C	s	t	u	v	n	C	s	t	u	v
1	0.00880496	0	0	0	0	1	0.003794	0	0	0	0
2	-0.20455400	1	0	0	0	2	0.008652	2	0	0	0
3	0.16635100	0	1	0	0	3	-0.03224	1	1	0	0
4	0.15811400	0	2	0	0	4	0.003448	0	2	0	0
5	-0.14758100	2	0	1	0	5	-0.04088	0	1	1	0
6	-0.48149700	1	1	1	0	6	-0.10801	1	1	1	0
7	0.41543700	0	2	1	0	7	-0.08854	2	1	1	0
8	0.01440430	0	0	0	1	8	0.188561	0	2	1	0
9	-0.05300540	2	0	0	1	9	-0.00371	1	0	0	1
10	0.01438810	0	1	0	1	10	0.005137	0	1	0	1
11	0.06068260	1	1	0	1	11	0.020945	1	1	0	1
12	-0.01258940	0	0	1	1	12	0.004743	2	1	0	1
13	0.01096890	1	0	1	1	13	-0.00723	2	0	1	1
14	-0.13369800	0	3	0	0	14	0.004438	1	1	1	1
15	0.00638407	0	6	0	0	15	-0.02694	0	2	1	1
16	-0.00132718	2	6	0	0	16	0.055808	3	0	1	0
17	0.16849600	3	0	1	0	17	0.016189	0	3	1	0
18	-0.0507214	0	0	2	0	18	0.003181	1	3	1	0
19	0.0854559	2	0	2	0	19	0.015896	0	0	2	0
20	-0.0504475	3	0	2	0	20	0.047173	1	0	2	0
21	0.010465	1	6	2	0	21	0.019628	3	0	2	0
22	-0.00648272	2	6	2	0	22	-0.05028	0	1	2	0
23	-0.00841728	0	3	0	1	23	-0.03002	3	1	2	0
24	0.0168424	1	3	0	1	24	0.041712	2	2	2	0
25	-0.0012296	3	3	0	1	25	-0.03977	0	3	2	0
26	-0.0317791	0	3	1	1	26	-0.0035	0	6	2	0
27	0.018604	1	0	2	1	27	-0.01069	3	0	0	1

28	-0.00410798	0	2	2	1	28	0.001109	3	3	0	1
29	-0.00060685	0	0	0	2	29	-0.00031	0	6	0	1
30	-0.0049819	1	0	0	2	30	0.003599	3	0	1	1
31	0.0025983	2	0	0	2	31	-0.00142	0	6	1	1
32	-0.00056053	3	0	0	2	32	-0.00384	1	0	2	1
33	-0.00163652	1	2	0	2	33	0.01268	0	2	2	1
34	-0.00032879	1	6	0	2	34	-0.00318	2	3	2	1
35	0.0001165	2	6	0	2	35	0.003343	0	6	2	1
36	0.0006909	0	0	1	2	36	-0.00183	1	1	0	2
37	0.00421749	0	3	1	2	37	0.000113	3	2	0	2
38	0.00005652	3	6	1	2	38	-3×10^{-5}	3	6	0	2
39	-0.00146564	0	3	2	2	39	0.00027	1	0	1	2
						40	0.000833	2	0	1	2
						41	0.001553	0	2	1	2
						42	0.000303	0	6	1	2
						43	-0.00018	0	0	2	2
						44	-0.00043	0	3	2	2
						45	8.69E-05	3	3	2	2
						46	-0.00047	0	6	2	2
						47	5.54E-05	1	6	2	2

Table 2.1: Coefficients for the polynomials form of K_T and K_Q

If the Reynolds Number of a particular design isn't fixed at 2×10^6 then a correction is necessary. Then corrections are added with the value of K_T and K_Q those are estimated by Eq.2.7 and Eq.2.8. Following two equations are used for calculating correction factor due to deviation of Reynolds Number from the standard Reynolds Number.

Correction for K_T :

2.9

$$\Delta K_T = 0.000353485$$

$$-0.00333758 \left(\frac{A_E}{A_0} \right) \cdot j^2$$

$$-0.00478125 \left(\frac{A_E}{A_0} \right) \cdot \left(\frac{P}{D} \right) \cdot j$$

$$+0.000257792 (\log R_n - 0.301)^2 \cdot \left(\frac{A_E}{A_0} \right) \cdot j^2$$

$$+0.0000643192 (\log R_n - 0.301) \cdot \left(\frac{P}{D} \right)^6 \cdot j^2$$

$$-0.0000110636 (\log R_n - 0.301)^2 \cdot \left(\frac{P}{D} \right)^6 \cdot j^2$$

$$-0.000276305 (\log R_n - 0.301)^2 \cdot Z \cdot \left(\frac{A_E}{A_0} \right) \cdot j^2$$

$$+0.0000954 (\log R_n - 0.301) \cdot Z \cdot \left(\frac{A_E}{A_0} \right) \cdot \left(\frac{P}{D} \right) \cdot J$$

$$+0.0000032049 (\log R_n - 0.301) \cdot Z^2 \cdot \left(\frac{A_E}{A_0} \right) \cdot \left(\frac{P}{D} \right)^3 \cdot J$$

Correction for K_Q :

$$\begin{aligned}
\Delta K_Q = & -0.000591412 \\
& +0.00696898 \frac{P}{D} \\
& -0.0000666654 \cdot Z \cdot \left(\frac{P}{D}\right)^6 \\
& +0.0160818 \left(\frac{A_E}{A_0}\right)^2 \\
& -0.000938091 (\log R_n - 0.301) \cdot \left(\frac{P}{D}\right) \\
& -0.00059593 (\log R_n - 0.301) \cdot \left(\frac{P}{D}\right)^2 \\
& +0.0000782099 (\log R_n - 0.301) \cdot 2 \left(\frac{P}{D}\right)^2 \\
& +0.0000052199 (\log R_n - 0.301) \cdot Z \cdot \left(\frac{A_E}{A_0}\right) \cdot J^2 \\
& -0.00000088528 (\log R_n - 0.301) \cdot 2Z \cdot \left(\frac{A_E}{A_0}\right) \cdot \frac{P}{D} \cdot J \\
& +0.0000230171 (\log R_n - 0.301) \cdot Z \cdot \left(\frac{P}{D}\right)^6 \\
& -0.00000184341 (\log R_n - 0.301) \cdot 2Z \cdot \left(\frac{P}{D}\right)^6 \\
& -0.00400252 (\log R_n - 0.301) \cdot \left(\frac{A_E}{A_0}\right)^2 \\
& +0.000220915 (\log R_n - 0.301) \cdot 2 \cdot \left(\frac{A_E}{A_0}\right)^2
\end{aligned} \tag{2.10}$$

2.3 Governing Equations

During the last decade considerable advances has been made in the application of the computational fluid dynamics to the analysis and design of the marine propellers. Several approaches for modelling the flow physics have been developed. Among them RANS (Reynold's Averaged Navier-Stokes) method has found most favor because the computational times are rather lower than for the other method. CFD methods are fundamentally based on the governing equations of fluid dynamics which represent mathematical enunciation of the conversation laws of physics. Following physical laws are associated in a CFD analysis.

Equation of Continuity:

$$\frac{\partial \rho}{\partial t} + \frac{\partial(\rho u_x)}{\partial x} + \frac{\partial(\rho u_y)}{\partial y} + \frac{\partial(\rho u_z)}{\partial z} = 0 \tag{2.11}$$

Conservation of momentum along X-axis:

$$\frac{\partial(\rho u_x)}{\partial t} + \nabla \cdot (\rho u_x u) = -\frac{\partial P}{\partial x} + \nabla \cdot (\mu \nabla u_x) + \rho g_x \quad 2.12$$

Conservation of momentum along Y-axis:

$$\frac{\partial(\rho u_y)}{\partial t} + \nabla \cdot (\rho u_y u) = -\frac{\partial P}{\partial y} + \nabla \cdot (\mu \nabla u_y) + \rho g_y \quad 2.13$$

Conservation of momentum along Z-axis:

$$\frac{\partial(\rho u_z)}{\partial t} + \nabla \cdot (\rho u_z u) = -\frac{\partial P}{\partial z} + \nabla \cdot (\mu \nabla u_z) + \rho g_z \quad 2.14$$

Equation of Turbulent Kinetic Energy (k):

$$\frac{\partial(\rho k)}{\partial t} + \frac{\partial(\rho k u_i)}{\partial x_i} = \frac{\partial}{\partial x_j} \left[\left(\mu + \frac{\mu_t}{\sigma_k} \right) \cdot \frac{\partial k}{\partial x_j} \right] + P_k + P_b - \rho \epsilon - Y_M + S_k \quad 2.15$$

Equation of Energy Dissipation (ϵ):

$$\frac{\partial(\rho \epsilon)}{\partial t} + \frac{\partial(\rho \epsilon u_i)}{\partial x_i} = \frac{\partial}{\partial x_j} \left[\left(\mu + \frac{\mu_t}{\sigma_k} \right) \cdot \frac{\partial \epsilon}{\partial x_j} \right] + C_{1\epsilon} \frac{\epsilon}{k} (P_k + C_{3\epsilon} P_b) - C_{2\epsilon} \rho \frac{\epsilon^2}{k} + S_\epsilon \quad 2.16$$

3 DESIGN AND ANALYSIS

Propeller design is critical for a ship's smooth operation. It is an iterative process. Nowadays, computer software is used to design propellers. The Wageningen B-series propeller, on the other hand, has a well-established polynomial regression formula that is simple to interpolate and optimize within the traditional propeller constraints. As a result, Wageningen B-series propeller geometries remain popular as a starting point for propeller design. So, Wageningen B-series geometry has been adapted here. Before beginning any calculations for the geometry of the propeller, the definition of the problem must be properly fixed.

3.1 Definition of the Problem

The definition of the problem is mainly the specification of the design points together with the constraints which are applicable to that design. There are two types of design problems for free running propellers.

1. Propeller diameter and the ship speed is given. Problem is to design the optimum propeller to minimize the power requirement and determine the optimum rpm.
2. Engine power and the rpm of the propeller is known, and the problem is to design the optimum propeller diameter that maximize the ship propulsive performance.

The problem of this thesis is of second type. The given parameters of the problem, their value and their unit are tabulated in the following table.

Problem Definition		
Parameter	Value	Unit
Ship speed, V_s	10	Knot
Ship length, L_{pp}	82.15	m
Breadth, B	13.69	m
Draft, T	4.28	m
Volume of displacement, ∇	3802	m^3
Brake power, P_B	1135	KW
Propeller RPM	393	-
Shaft efficiency, η_s	0.98	-

Table 3.1: Problem Specification

3.2 Design

For finding the optimum values of open water characteristics of the propeller total resistance is calculated using Holtrop and Mennen (**Appendix A**) method. The blade number is an important parameter for propeller-induced vibration. Odd numbered propeller has better vibration characteristics than even numbered propeller. High blade number reduce vibration problems but increase manufacturing costs. Blade number, $Z = 3$ is optimized for most of the design problems. Delivered power, thrust and torque (**Appendix C**) of the propeller is given as follows.

Resistance, R_T	92.63 kW
Number of blades, Z	3
Thrust, T	102.02 kN
Delivered Power, P_D	945.45 kW
Torque, Q	945.45 kN – m

Table 3.2: Design Constraints

K_T and K_Q values are calculated using regression formula for different pitch ratio $\left(\frac{P}{D}\right)$.

$$\begin{Bmatrix} K_T(R_n) \\ K_Q(R_n) \end{Bmatrix} = \begin{Bmatrix} K_T(R_n = 2 \times 10^6) \\ K_Q(R_n = 2 \times 10^6) \end{Bmatrix} + \begin{Bmatrix} \Delta K_T(R_n) \\ \Delta K_Q(R_n) \end{Bmatrix} \quad 3.1$$

For simplicity of the calculation, Reynold's Number (R_N) is taken as 2×10^6 . Hence, there is no correction in the values of K_T and K_Q . As Wageningen-B series propeller is used all the necessary polynomial coefficients are taken from standard series data of the Wageningen -B series propeller as shown in **Table 2.1**.

$\left(\frac{A_E}{A_0}\right)$ is required to determine K_T and K_Q values using Eq.2.7 and Eq.2.8. So, $\left(\frac{A_E}{A_0}\right)$ is determined using Keller formula as follows.

$$\frac{A_E}{A_0} = \frac{(1.3 + 0.3Z)T}{(P_0 - P_V) \cdot D^2} + K \quad 3.2$$

Here the value of K varies with number of propeller and ship type. $K = 0.2$ for single screw ship.

Pitch ratios are taken greater than 0.6 as optimum efficiency of the propeller typically achieved at pitch ratio between 0.6 and 1.2. Open water diagram is obtained after calculating open water characteristics at a particular pitch ratio over different advance coefficient.

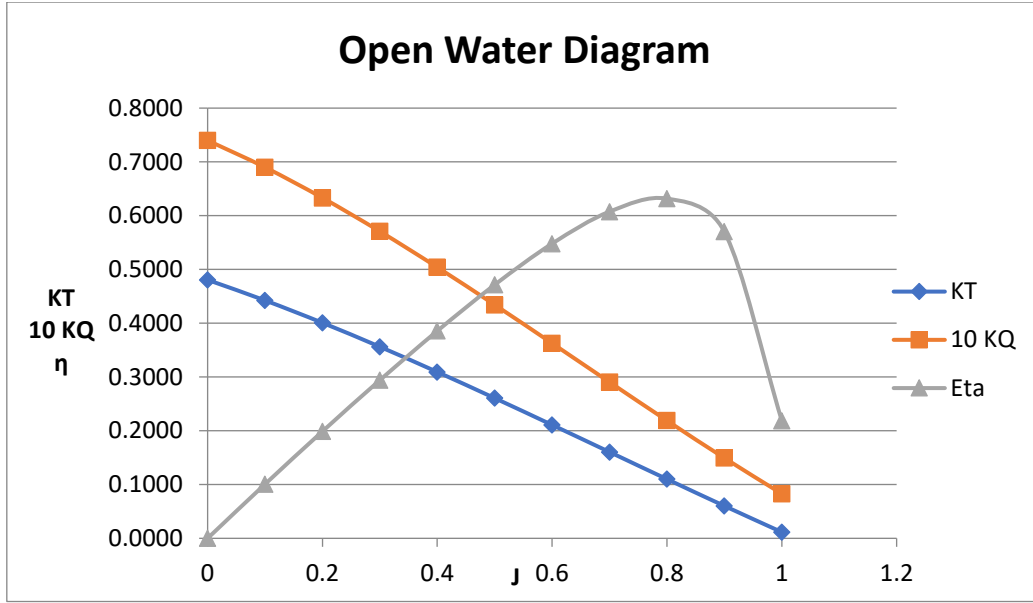


Figure 3.1: Open water diagram for pitch ratio 1.0

As the delivered power is given, K_Q can be calculated for different values of J using Eq.2.4. Velocity of advance is required in this calculation. So, the velocity of advance is calculated using the Eq.2.5. For determining the velocity of advance wake fraction is necessary. Wake fraction is determined using the equation of Taylor wake fraction (**Appendix B**) in which diameter of the propeller is required. Diameter is estimated using the following empirical equation.

$$D_{max} = D_B = a \cdot T \quad 3.3$$

Where, $a < 0.65$ for bulk carriers and tankers.

J	D	K _Q
0.0001	6566.4992	4.38598E-20
0.1	6.5665	0.00004
0.2	3.2832	0.00140
0.3	2.1888	0.01066
0.4	1.6416	0.04491
0.5	1.3133	0.13706
0.6	1.0944	0.34105
0.7	0.9381	0.73715
0.8	0.8208	1.43720
0.9	0.7296	2.58988
1	0.6566	4.38598

Table 3.3: K_Q for different J values for fixed P_D

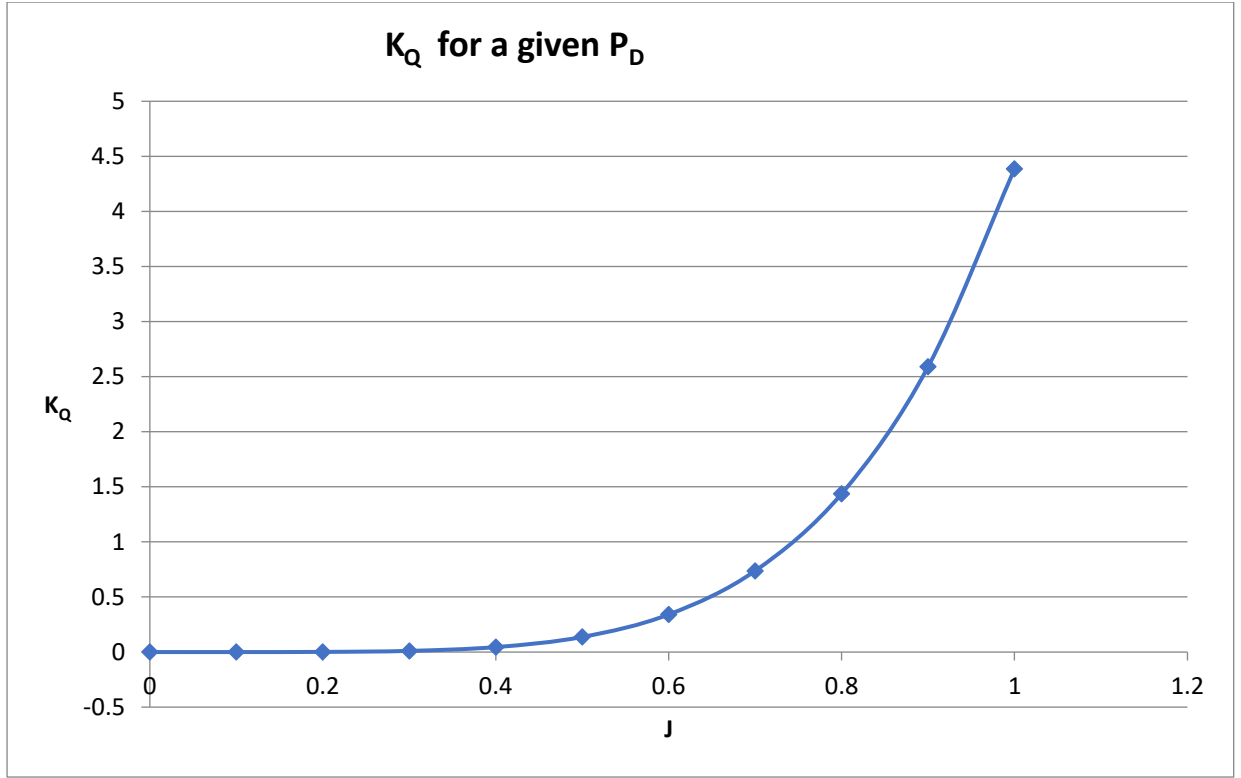


Figure 3.2: K_Q over advance coefficient for given P_D

K_Q over J plot for different pitch ratio is then plotted on the graph **Figure 3.2** to find the intersections. Intersection points are the optimum operating point for that given pitch ratio.

J	K _Q			
	P/D = 0.6	P/D = 0.8	P/D = 1	P/D = 1.2
0.0001	0.02515	0.04609	0.07399	0.10761
0.1	0.02261	0.04228	0.06899	0.10154
0.2	0.01963	0.03790	0.06331	0.09470
0.3	0.01636	0.03308	0.05708	0.08720
0.4	0.01295	0.02795	0.05041	0.07917
0.5	0.00956	0.02267	0.04343	0.07071
0.6	0.00635	0.01736	0.03627	0.06194
0.7	0.00346	0.01216	0.02905	0.05299
0.8	0.00106	0.00721	0.02189	0.04396
0.9	-0.00071	0.00265	0.01493	0.03498
1	-0.00169	-0.00139	0.00829	0.02615

Table 3.4: K_Q for different pitch ratio

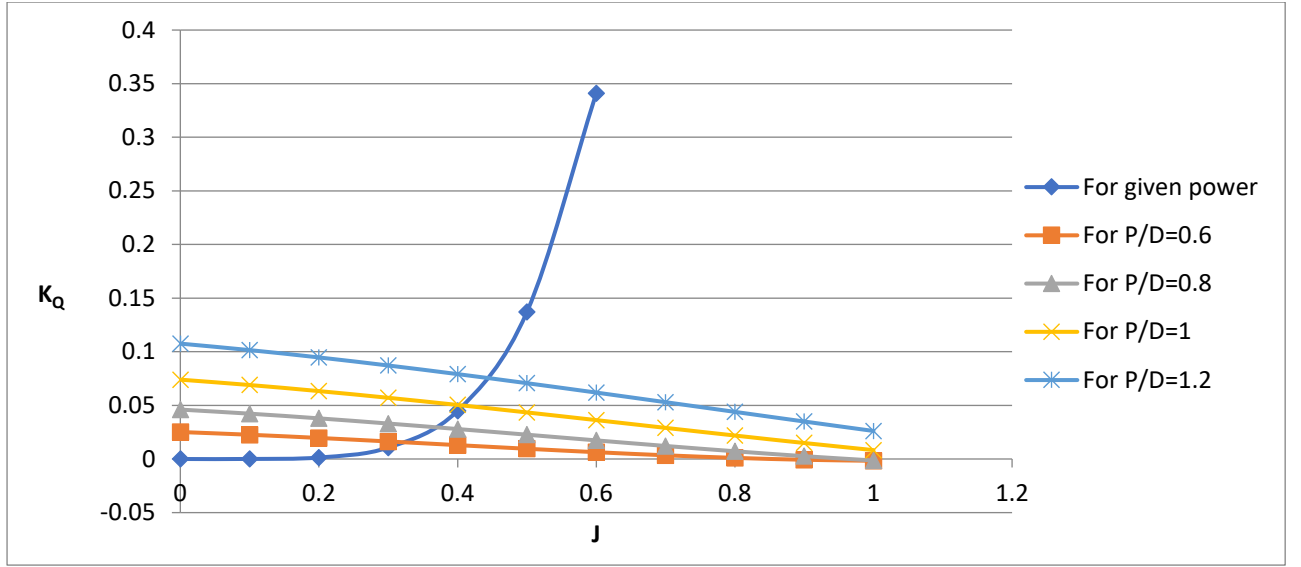


Figure 3.3: K_Q Intersection for different pitch ratio

From the above graph, intersection data points are taken. K_T is obtained in a very similar way of K_Q . Then using the Eq.2.6 open water efficiency is calculated as shown in the table below.

	J1	J2	J3	J4
$\frac{P}{D}$	0.6	0.8	1	1.2
J	0.3232	0.3678	0.4082	0.4433
K_T	0.12560	0.21341	0.30542	0.39968
K_Q	0.01557	0.02963	0.04984	0.07555
η_0	0.40946	0.41615	0.39290	0.36839

Table 3.5: Intersection data points

The open water efficiency is then plotted against advance coefficient using the data of the table above.

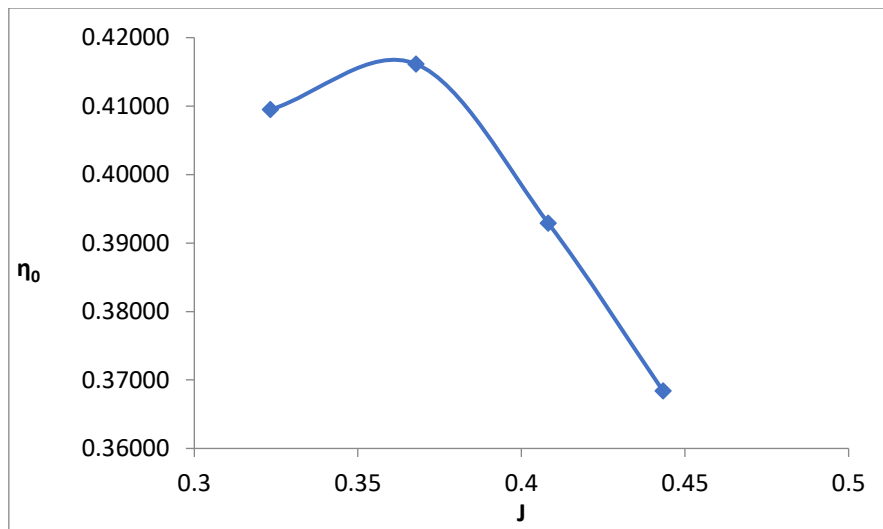


Figure 3.4: Maximum open water efficiency

From the above graph, the optimum open water efficiency and advance coefficient are obtained. Corresponding optimum values of K_T , K_Q and pitch ratio are obtained by interpolating on the data of **Table 3.5**. The optimum diameter is obtained using the equation Eq.2.3.

Optimum values		
J_{OPT}	0.36	From graph
η_0	0.42	From graph
D_{OPT}	1.83	m
P/D	0.76	By interpolation
P	1.39	

Table 3.6: Optimum Values

Polynomial regression is carried out one more time using the optimum values to observe how thrust and torque coefficient varied with the changes of advance coefficient. The results are shown in the table below.

J	K_T	K_Q	$10K_Q$	$\eta_0 = \frac{J}{2\pi} \cdot \frac{K_T}{K_Q}$
0.0001	0.3370	0.0413	0.4132	0.0001
0.1	0.3016	0.0378	0.3776	0.1255
0.2	0.2628	0.0336	0.3365	0.2454
0.3	0.2212	0.0291	0.2912	0.3578
0.4	0.1773	0.0243	0.2433	0.4578
0.5	0.1318	0.0194	0.1941	0.5333
0.6	0.0852	0.0145	0.1450	0.5541
0.7	0.0382	0.0097	0.0974	0.4319
0.8	-0.0086	0.0053	0.0527	-0.2053
0.9	-0.0547	0.0012	0.0123	-6.2807
1	-0.0995	-0.0022	-0.0223	7.0022

Table 3.7: Open water data for optimum pitch ratio

Open water diagram is drawn based on the data in the **Table 3.7**.

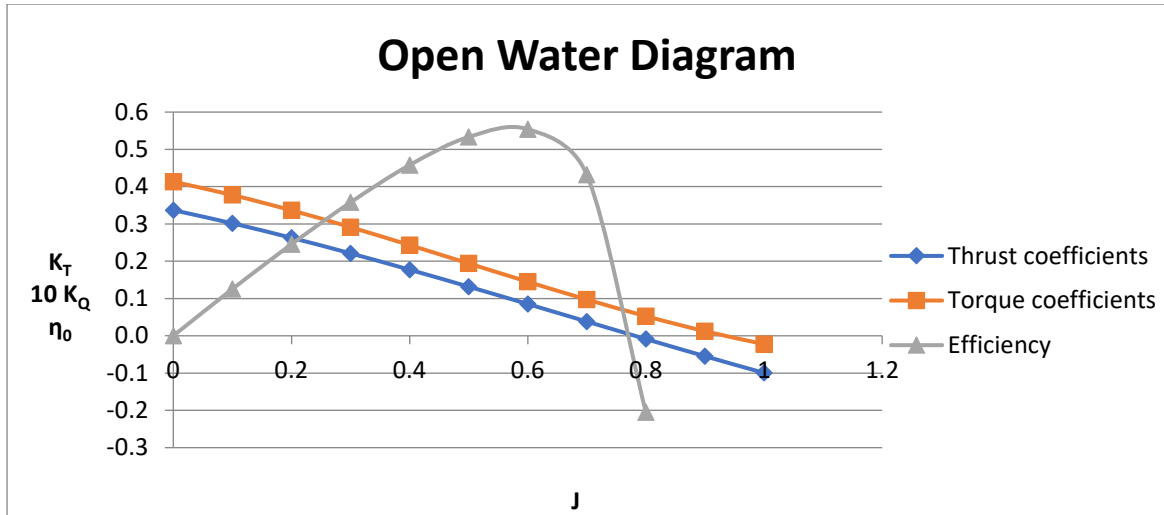


Figure 3.5: Open water diagram for optimum pitch ratio

3.3 Geometry Generation

The coordinates of the Wageningen-B series propeller for the chosen design are calculated (**Appendix D**). Using the coordinates, 3D geometry is constructed in the software **PropCad**. It has made the geometry generation easier by considering the rake and skew angle. But this 3D geometry is not yet ready for simulation because some modifications are needed like-joining of the blades and hub, smothering of the joints etc. Those are easily done by using the software **Rhinoceros**.

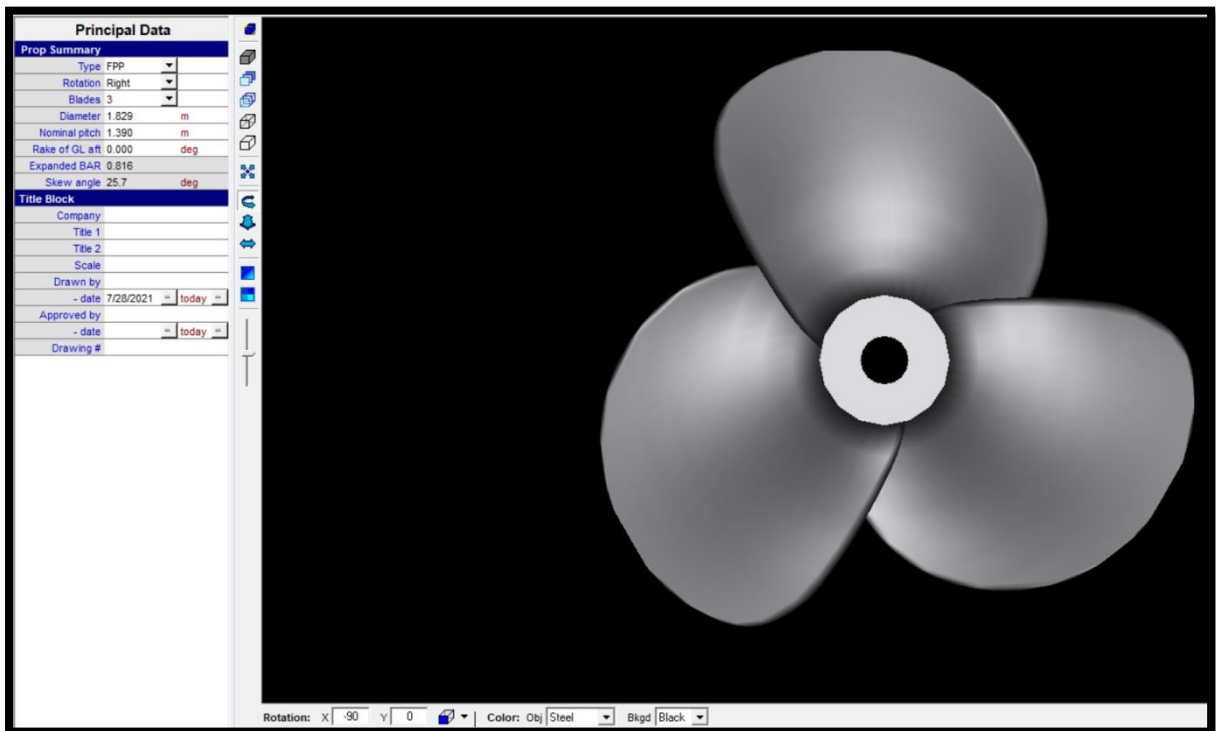


Figure 3.6: Geometry of the propeller in PropCad

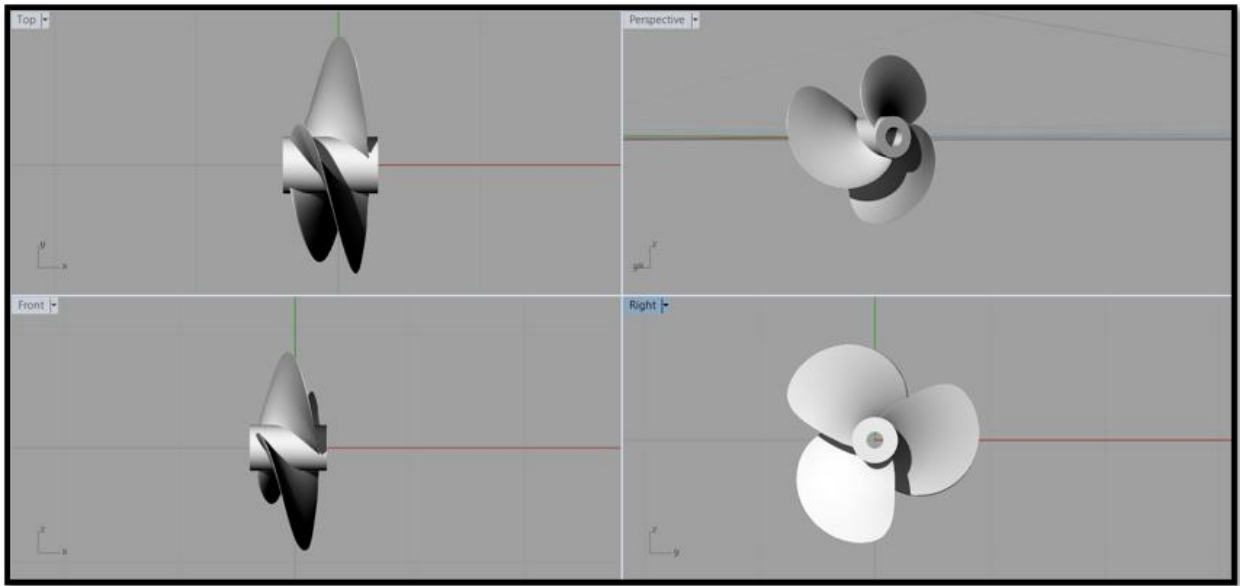


Figure 3.7: 3D model of the propeller in **Rhinoceros**

A shroud is designed for the ducted propeller. Conventional propeller already designed is then fitted with the shroud. The shroud chosen here is the standard 19A duct (**Appendix E**) because it is the most common type.

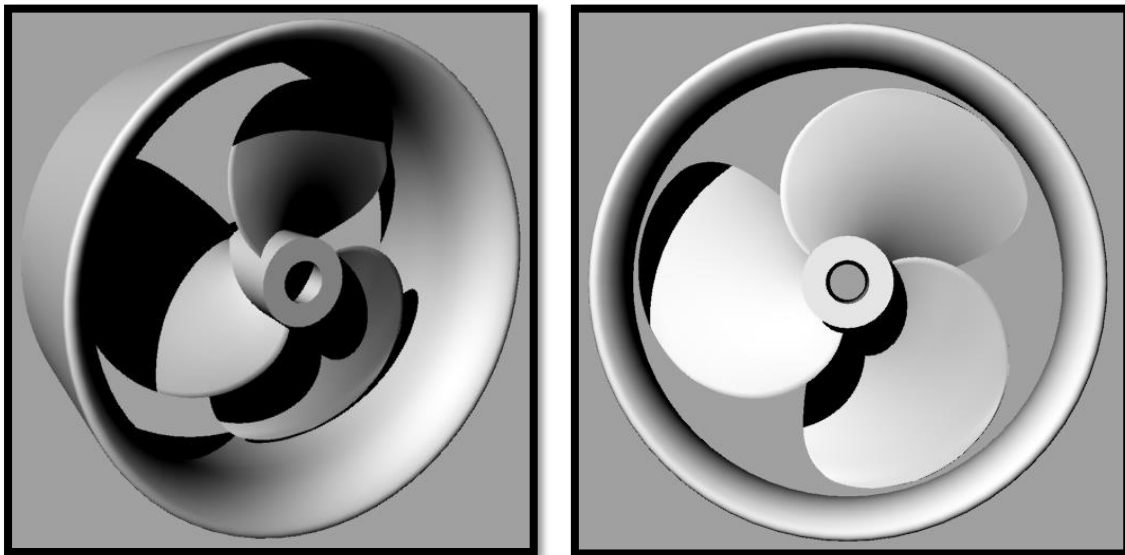


Figure 3.8: Ducted propeller model in **Rhinoceros**

3.4 Analysis

Numerical Analysis of the propeller is carried out in Ansys (Fluent). But before the 3D fluid flow simulation around the propeller the geometry is imported in the Ansys software.

3.4.1 Domain

Generated geometry of the propeller using Wagnerian-B series screw propeller data is imported in Fluent. There are two type of domain is used here.

- Stationary Domain
- Rotary Domain

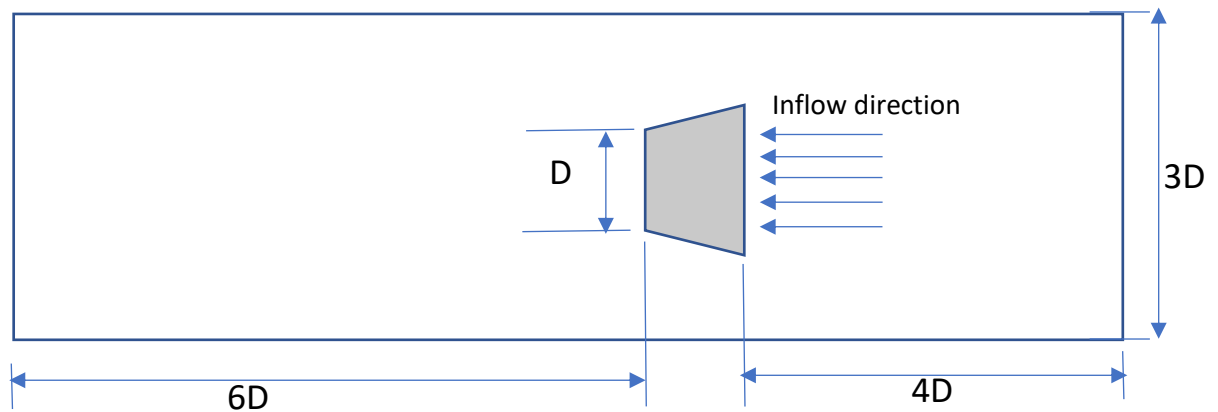


Figure 3.9: Scheme of the propeller and fluid domain

Both the stationary and the rotary domain are cylindrical. Upstream length is taken as **4D**, and the downstream length is taken as **6D**. The zone diameter is **3D** as shown in the **Figure 3.9**. Where, **D** is the diameter of the propeller. These dimensions are same for both the conventional and ducted propeller systems.

3.4.2 Boolean

Boolean is used to add and subtract different solid. Two Boolean subtract has been done for the simulation purposes. For the conventional propeller:

First Boolean subtract includes-

Tool body: Propeller

Target body: Rotary domain

Preserve: No

Second Boolean subtract includes-

Tool body: Rotary domain

Target body: Static domain

Preserve: Yes

For the ducted propeller the only difference is in the tool body of first Boolean subtract. Both the propeller and duct are selected here.

3.4.3 Meshing

Before the fluid flow simulation around the propeller meshing must be done properly. Discretization of the rotary and static domain is done by FVM (Finite Volume Method). Tetrahedral element is used here. Both global and local meshing has been done. Local meshing has been applied at the propeller (in case of ducted propeller in duct too) with smaller cell size due to complex shape to get better results. All the parameters considered and applied are shown.

Details of “Mesh”			
Display		Quality	
Display Style	Use Geometry Setting	Check Mesh Quality	Yes, Errors
Defaults		Target Skewness	0.9 (default)
Physics Preference	CFD	Smoothing	High
Solver Preference	Fluent	Mesh Metric	None
Element Order	Quadratic	Inflation	
Element Size	200 mm	Use Automatic Inflation	None
Export Format	Standard	Inflation Option	Smooth Transition
Export Preview Surface Mesh	No	Transition Ratio	0.272
Sizing		Maximum Layers	5
Use Adaptive Sizing	No	Growth Rate	1.2
Growth Rate	1.2 (default)	Inflation Algorithm	Pre
Max. Size	300 mm	View Advanced Options	No
Mesh Defeaturing	Yes	Assembly Meshing	
Defeature Size	1 mm (default)	Method	None
Capture Curvature	Yes	Advanced	
Curvature Min. Size	10 mm	Number of CPUs for parallel...	Program Controlled
Curvature Normal Angle	20°	Straight Sided Elements	No
Capture Proximity	Yes	Rigid Body Behavior	Dimensionally Reduced
Proximity Min. Size	10 mm	Triangle Surface Mesher	Program Controlled
Num. Cells Across Gap	3 (default)	Tropology Checking	Yes
Proximity Size Function Sou.	Faces and Edges	Pinch Tolerance	9 mm (default)
Bounding Box Diagonals	22699 mm	Generate Pinch on Refresh	No
Average Surface Area	2.2619e+007 mm ²	Statistics	
Minimum Edge Length	2.2781 mm	Nodes	2341817
		Elements	1677098

Table 3.8: Details of meshing

Details of “Face Sizing”-Sizing	
Scope	
Scoping Method	Geometry Selection
Geometry	18 Faces
Definition	
Suppressed	No
Type	Element Size
Element Size	20 mm
Advanced	
Defeature Size	1 mm (default)
Growth Rate	1.2 (default)
Capture Curvature	Yes
Curvature Normal Angle	20°
Local Min. Size	5 mm
Capture Proximity	Yes
Proximity Min. Size	5 mm
Num. Cells Across Gap	3 (default)
Proximity Size Function Sources	Faces and Edges

Table 3.9: Details of Sizing

Details of “Patch Conforming Method”-Method	
Scope	
Scoping Method	Geometry Selection
Geometry	1 Body
Definition	
Suppressed	No
Method	Tetrahedrons
Algorithm	Patch Conforming
Element Order	Quadratic

Table 3.10: Details of Method

The division of nodes and elements in static and rotary domain are shown below-

- Total nodes = 2341817 (Rotary-1687442, Static-654375)
- Total elements = 1677098 (Rotary-1212725, Static-464373)

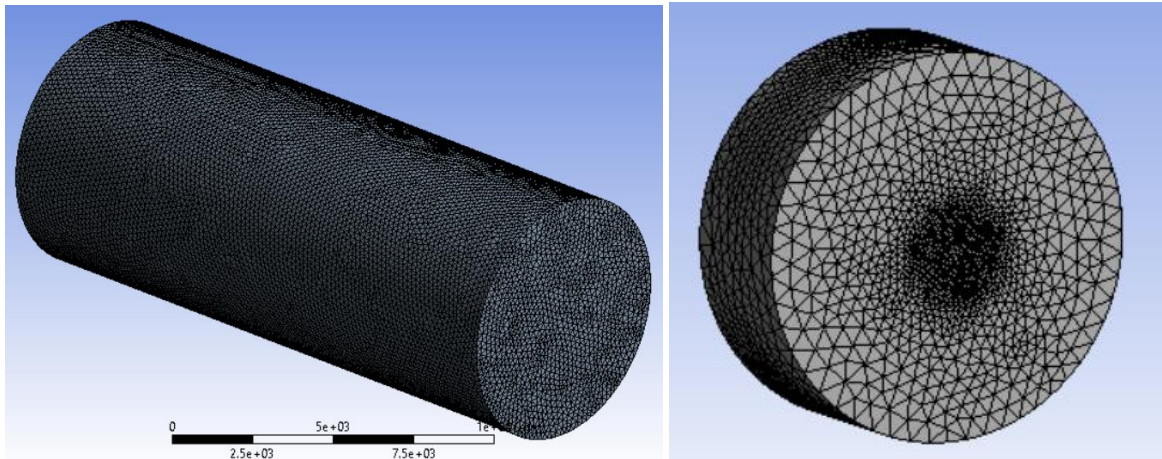


Figure 3.10: Meshing of Static and Rotary Domain (Conventional)

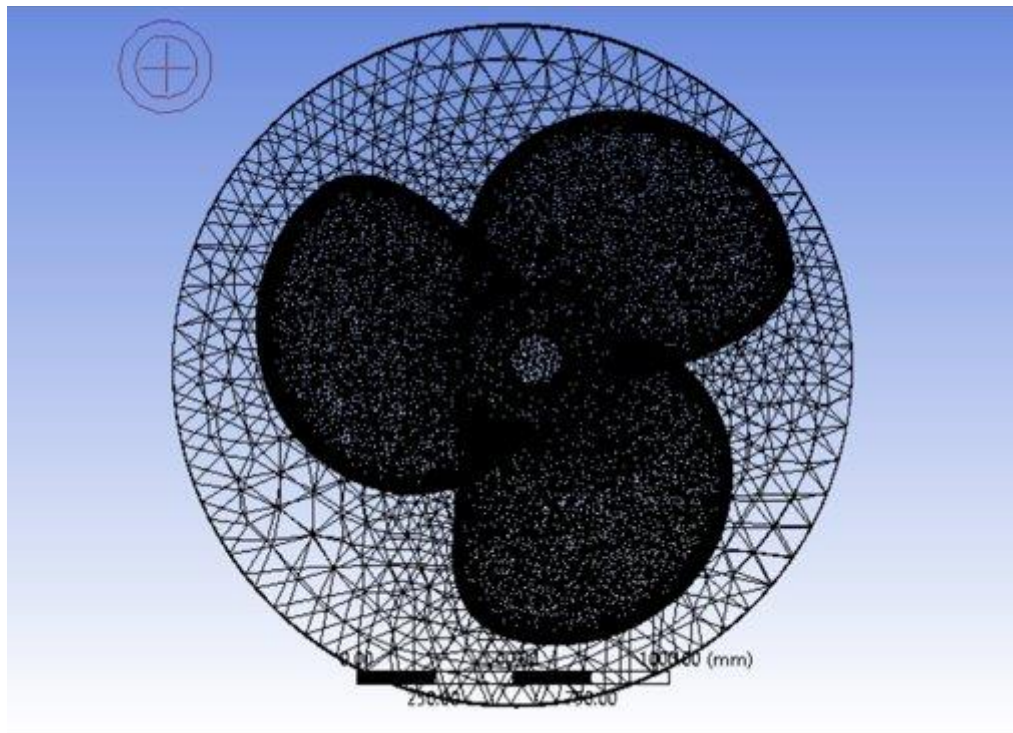


Figure 3.11: Meshing of the propeller(conventional)

This figure shows the meshing view of the propeller in wireframe. Due to complex shape of the propeller smaller cell size, patch conforming method, capture curvature and proximity have been applied in the rotary domain which has enabled better capture at the leading edge, trailing edge, tips etc. And for that reason, the number of elements and nodes is higher in rotary domain than the static domain.

Grid convergence test is done by varying the element size of the propeller from 15mm to 60mm and observing the change in the result of K_T , $10K_Q$ and Open water efficiency, η_0 .

Element size in mm	Total number of elements	% Error K_T	% Error $10K_Q$	% Error η_0
15	1910315	4.4117	9.7078	5.8655
20	1677098	4.1578	10.0726	6.5773
25	1586888	3.7780	10.3093	7.2821
30	1546380	3.9821	10.7350	7.5650
40	1515127	3.8470	11.0408	8.0867
60	1502253	3.7629	11.1956	8.3698

Table 3.11: Mesh sensitivity analysis

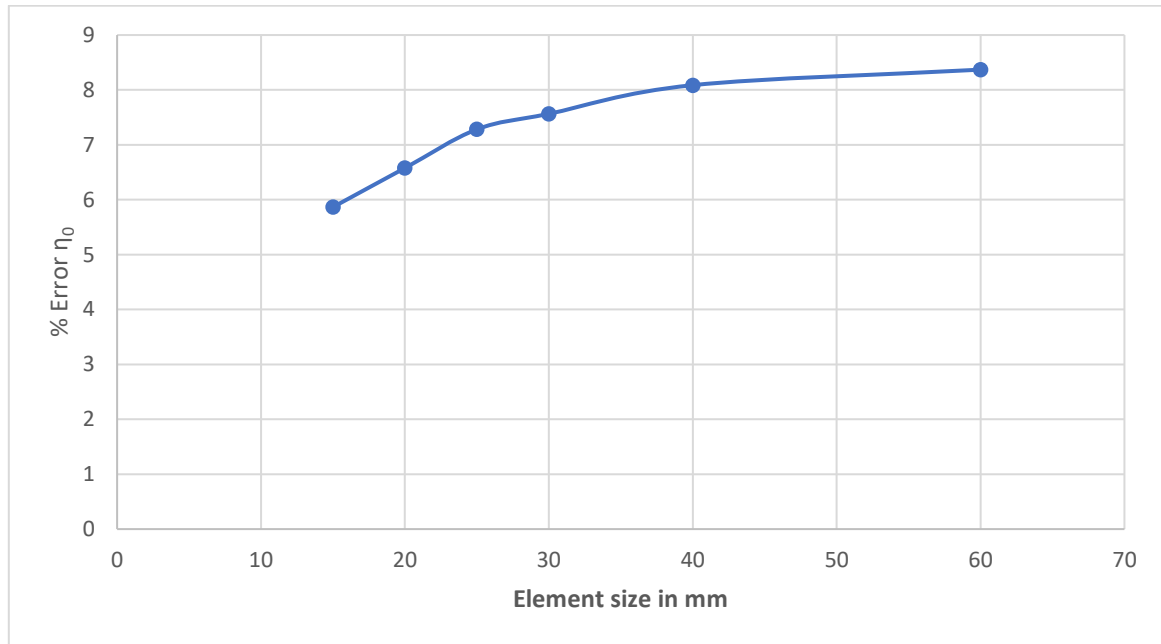


Figure 3.12: Mesh convergence

Reduction in size of the element reduces the error percentage of open water efficiency. Least percentage of error is observed in element size 15mm, but the simulation time is greater than other element sizes here. Since the result does not vary significantly after reduction of element size below 25mm we chose 20mm element size for our simulation since it gives quite reasonable error percentage in reasonable simulation time.

Same input parameters have been used for meshing of the ducted propeller and there is only difference in statistics which shows-

Total nodes: 4474012 (Rotary-3786808, Static-687204)

Total elements: 3180289 (Rotary-2692626, Static-487663)

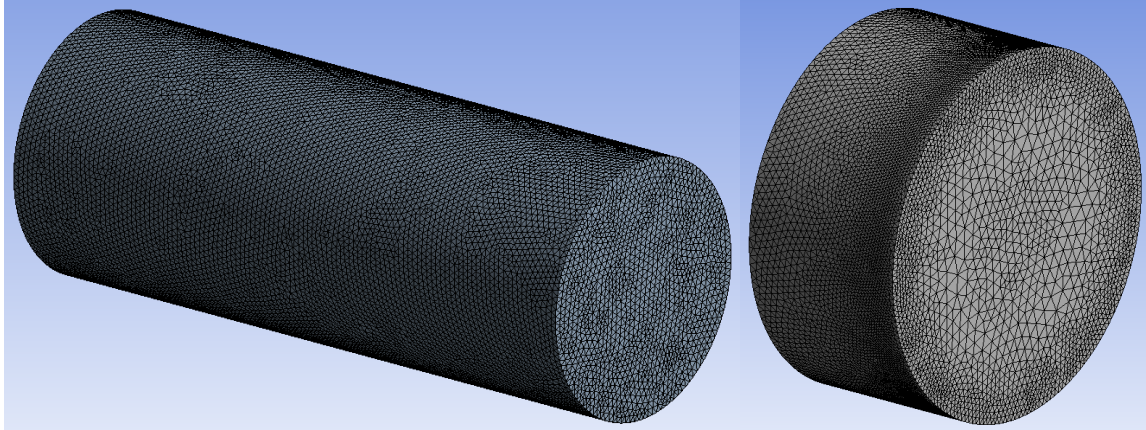


Figure 3.13: Meshing of Static and Rotary Domain (Ducted)

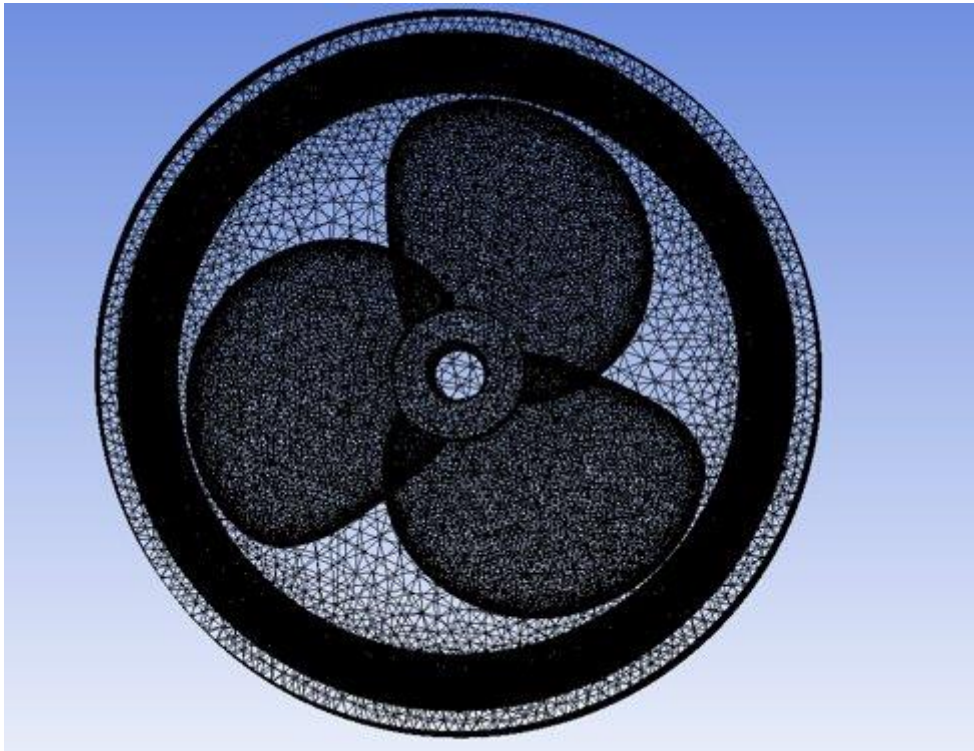


Figure 3.14: Meshing of propeller and duct

3.4.4 Setup & Simulation

The solver used here is Pressure Based with Implicit formulation of linearization. There are three types of boundary conditions used here: the velocity inlet, pressure outlet and taking the propeller surface as Stationary Wall with No slip Shear condition.

The velocity formulation type is absolute not relative, and we are considering the transient case not steady.

The viscous effect is considered here. As we are working with k-epsilon realizable turbulent model, it then must be selected.

The propeller normally works in water which indicates single phase. So, the multiphase function must be made off here.

In the fluid zone, the Frame Motion has been applied where the propeller is stationary and the fluid will move rotating at an angular speed of 393 rpm. This is also referred as moving reference frame.

SIMPLE algorithm has been chosen as the pressure-velocity method. Discretization method for pressure is second order and for momentum, turbulent kinetic energy, turbulent dissipation rate is second order upwind.

Hybrid Initialization has been chosen as the initialization method.

In case of ducted propeller, there are two changes-

1. The duct is on no slip wall boundary condition
2. Instead of Frame Motion, Mesh Motion has been applied here

After following all the steps (**Appendix F**), the simulation is run and checked for the results to converge. It is ensured by the residuals and thrust force convergence.

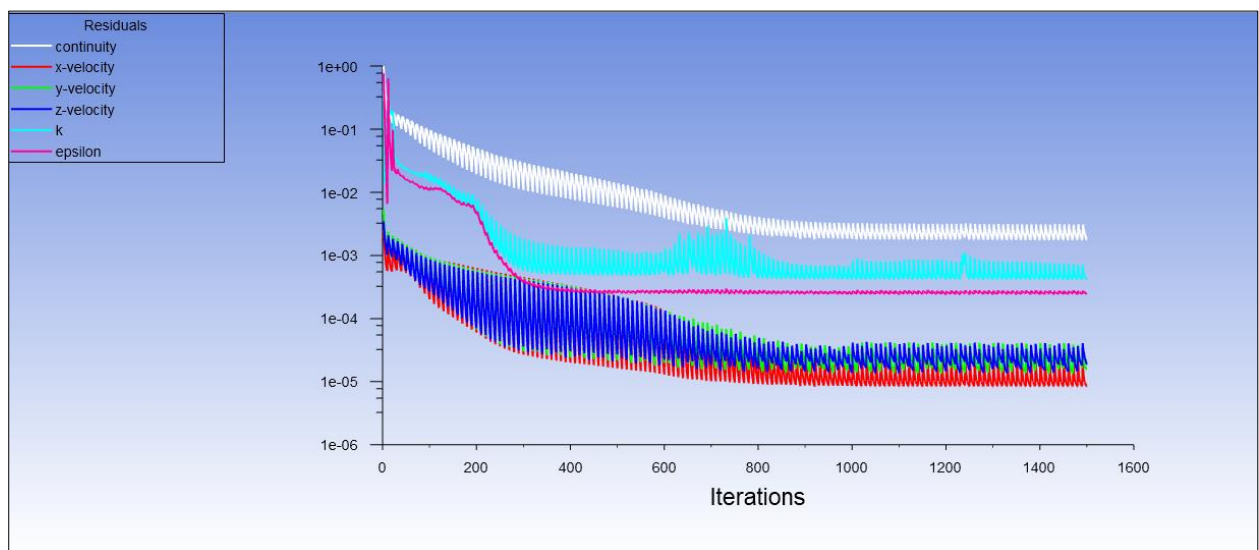


Figure 3.15: Residuals (conventional, $J=0.6$)

We know, all calculations are done for the centroid of the individual cell. And the residuals are the force or energy imbalances for the cells which are then globally calculated. When these residuals are zero, the exact results are obtained but this is very difficult to achieve, and it is tried to keep them as small as possible. For these obtained results, we can see that the residuals are not changing after 850 iterations. So, here the result has converged, and the figure shows the minimum residuals for this case.

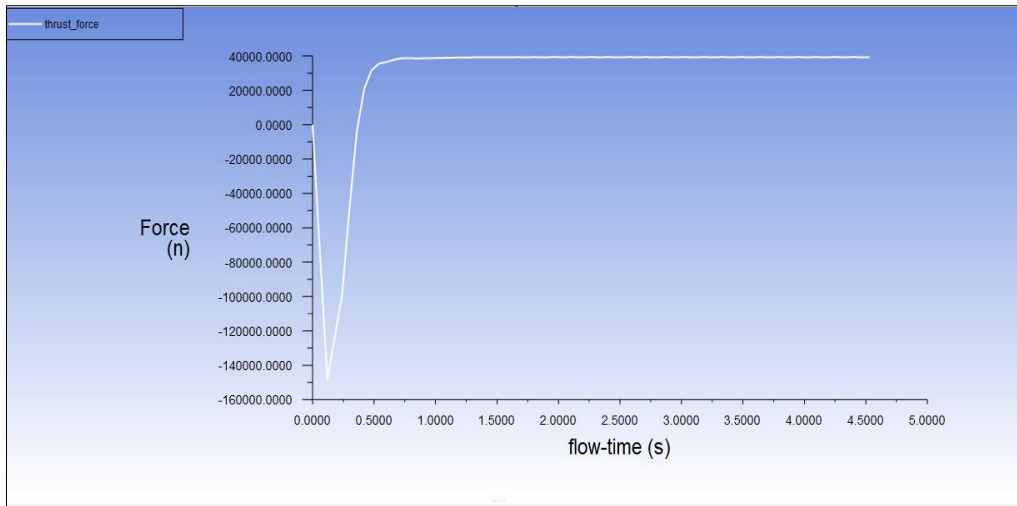


Figure 3.16: Thrust force (conventional, $J=0.6$)

The thrust force is observed against the flow time. Here, we can see that the thrust force has converged after 1 second of flow time and the figure shows the obtained thrust force for advance coefficient of 0.6

The following parameters are also observed-

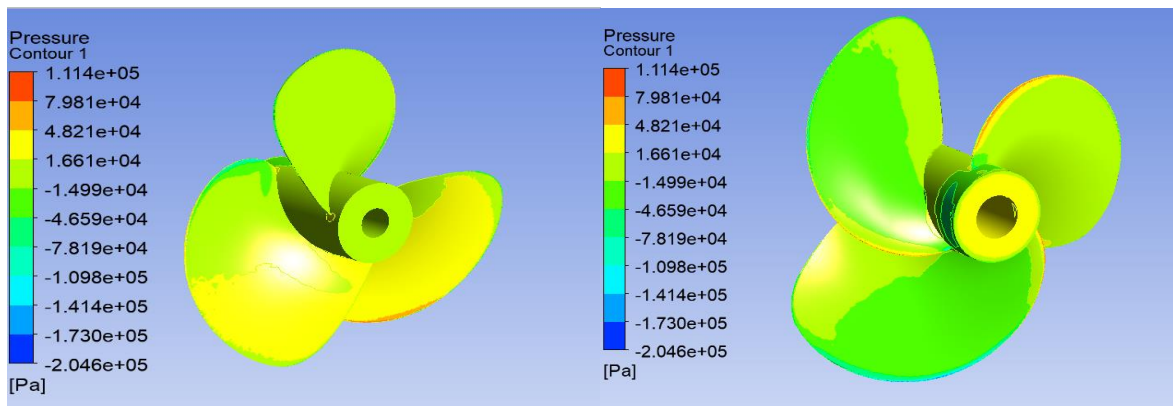


Figure 3.17: Pressure contour (conventional, $J=0.6$)

The figure shows a higher pressure at the leading edge of the blade. The blade face has comparatively higher pressure than the back side of the blade.

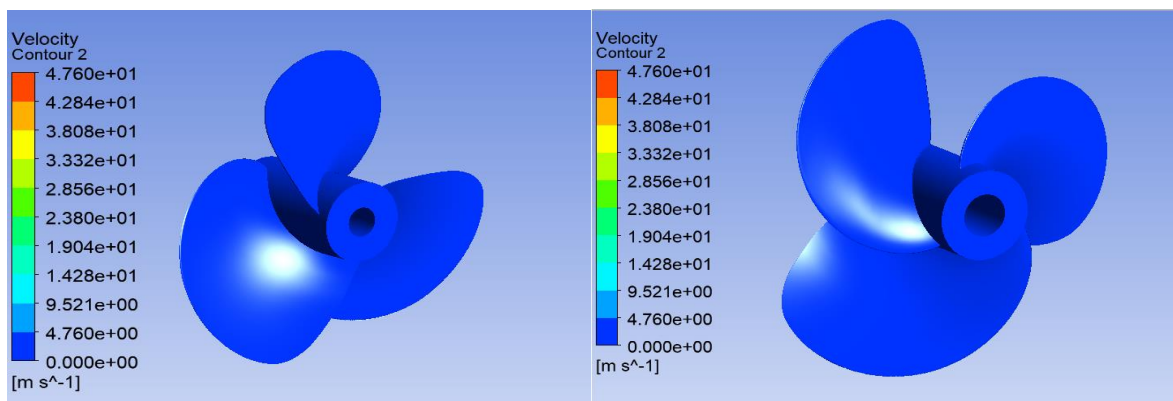


Figure 3.18: Velocity contour (conventional, $J=0.6$)

This figure shows zero velocity at the propeller. Because moving reference frame has been applied where the propeller is stationary.

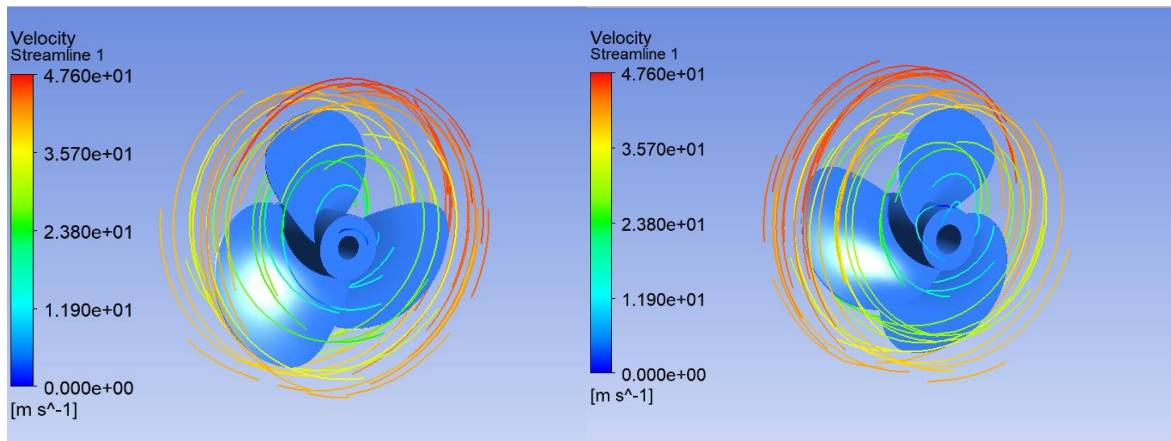


Figure 3.19: Velocity streamlines (conventional, $J=0.6$)

Here we can see that the velocity increases from the hub towards the tip of the blades.

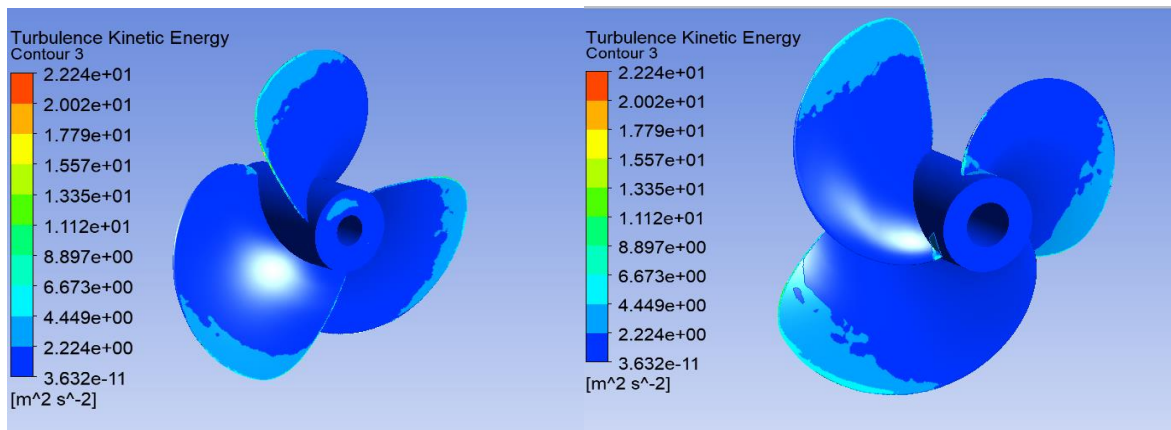


Figure 3.20: Turbulence kinetic energy (conventional, $J=0.6$)

This figure shows that the turbulent kinetic energy is higher at the tip of the blades and their adjacent areas at both face and backside. The other areas show no effect.

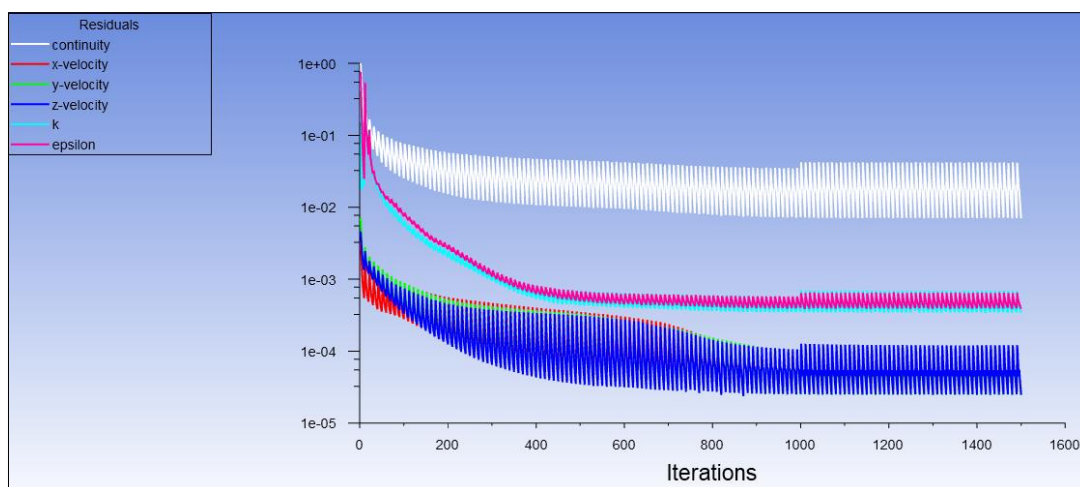


Figure 3.21: Residuals (ducted, $J=0.5$)

Here, the figure shows that the residuals have converged after 1000 iterations.

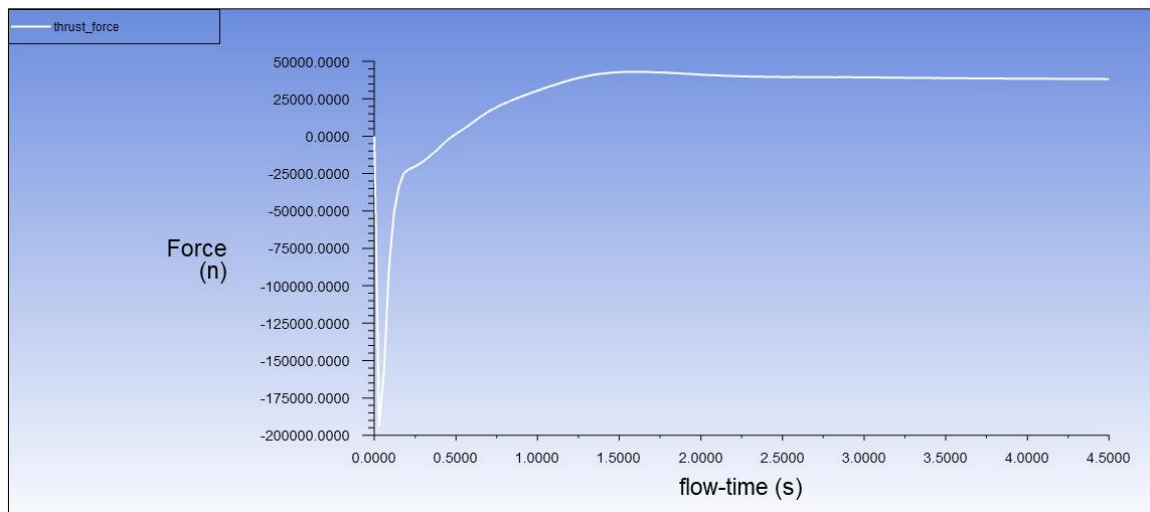


Figure 3.22: Thrust force (ducted, $J=0.5$)

Here, the figure shows that the thrust force has converged after 2.5 second of flow time.

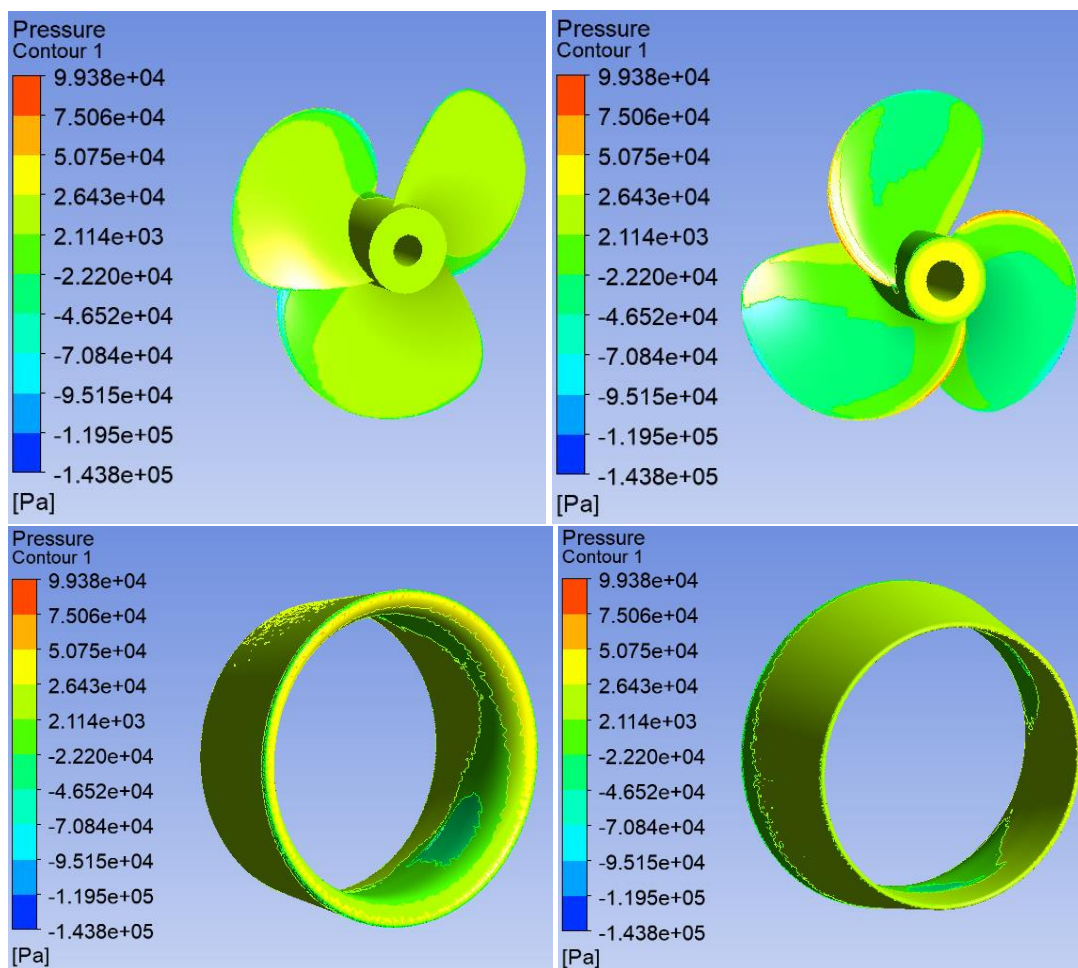


Figure 3.23: Pressure contour (ducted, $J=0.5$)

The highest pressure is at the leading edge of the blades and the faces are showing comparatively higher pressure than the backside. The duct is showing some lower pressures at some areas. Actually the duct has created negative pressure at this speed range.

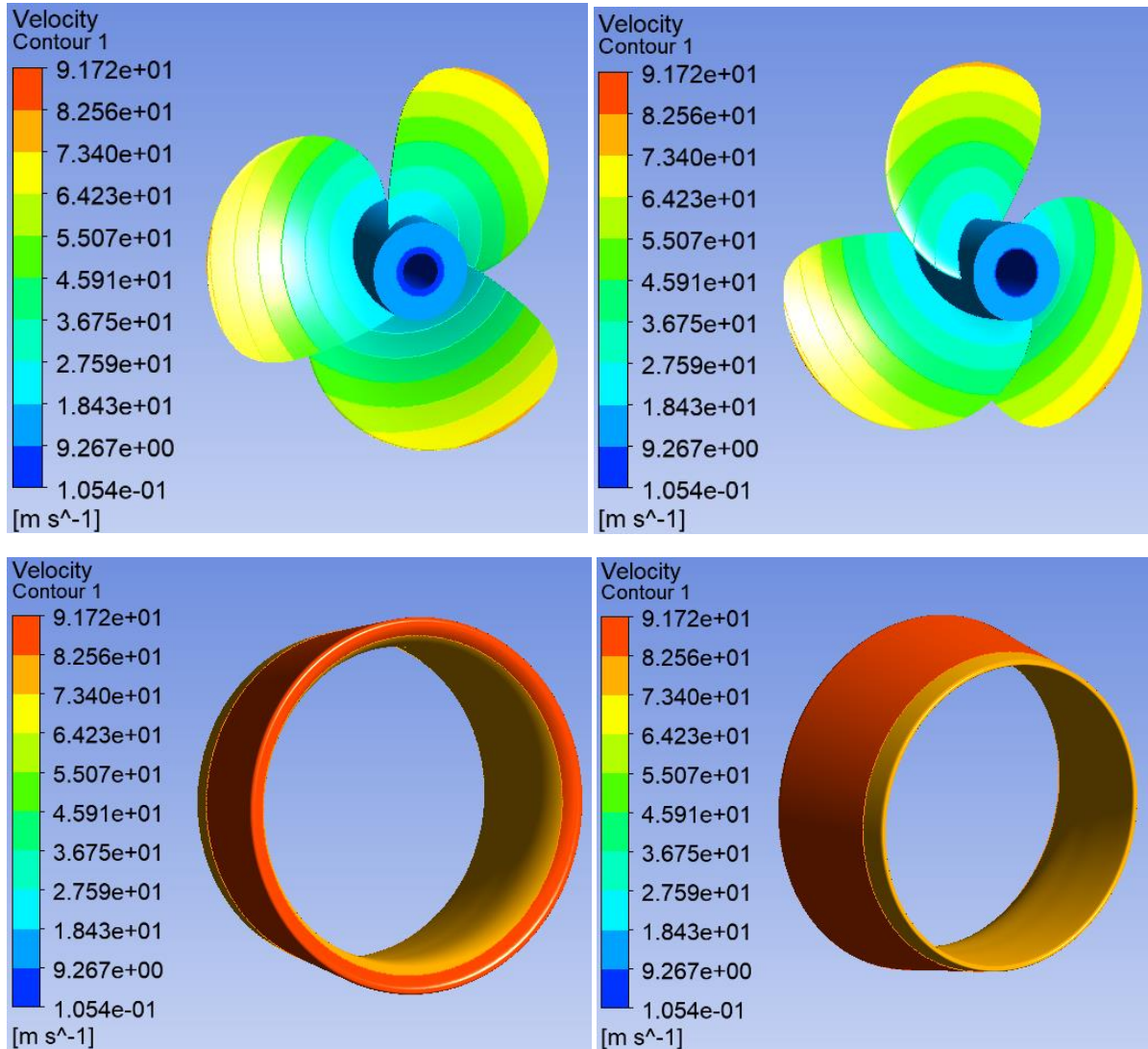


Figure 3.24: Velocity contour (ducted, $J=0.5$)

This figure shows the distribution of velocity at different radial positions because mesh motion has been applied here and in mesh motion the propeller and duct are not stationary. The velocity increases from the position of hub towards the blade tips and the velocity is highest at the position of the duct.

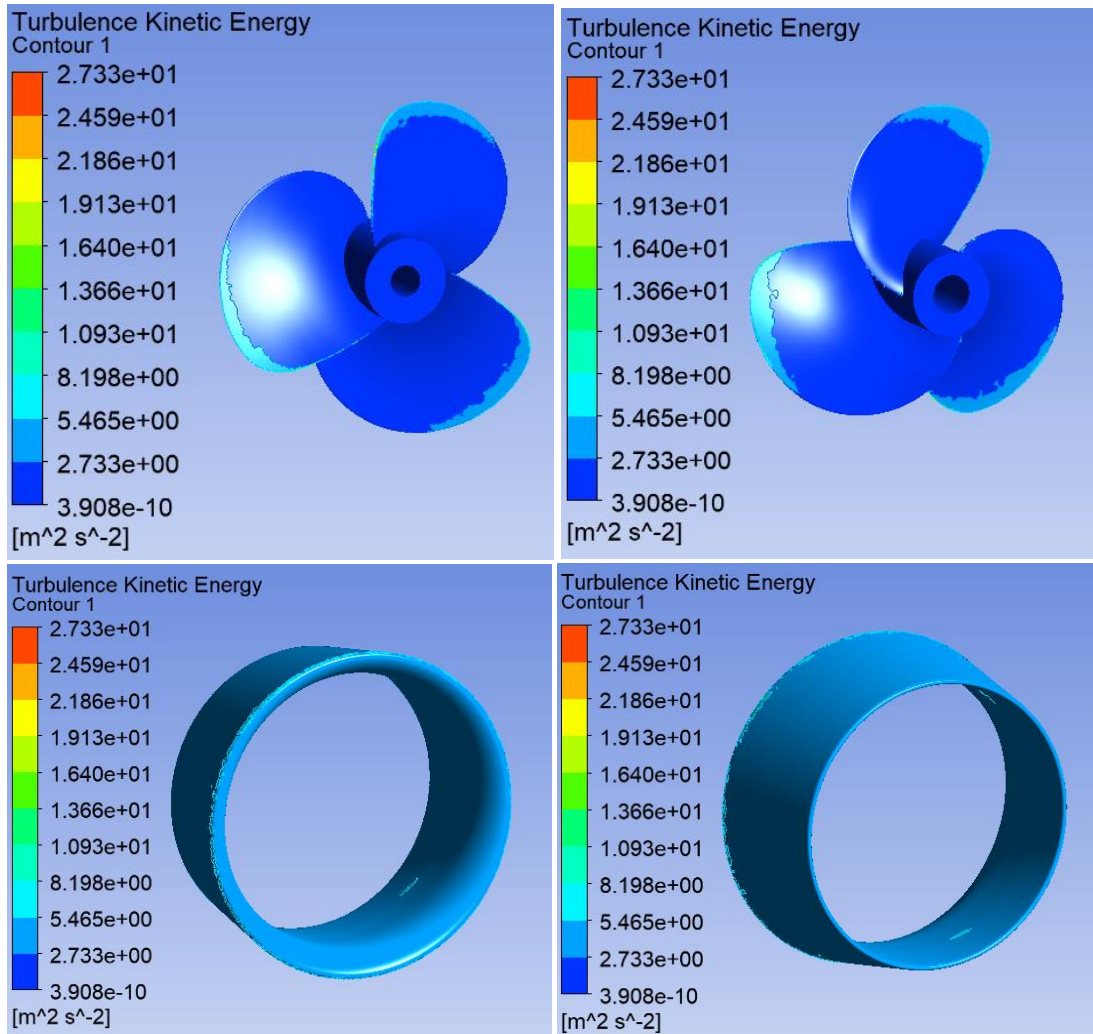


Figure 3.25: Turbulence kinetic energy (ducted, $J=0.5$)

The blade tips and the duct are showing higher turbulence kinetic energy compared to the other portion of the propeller.

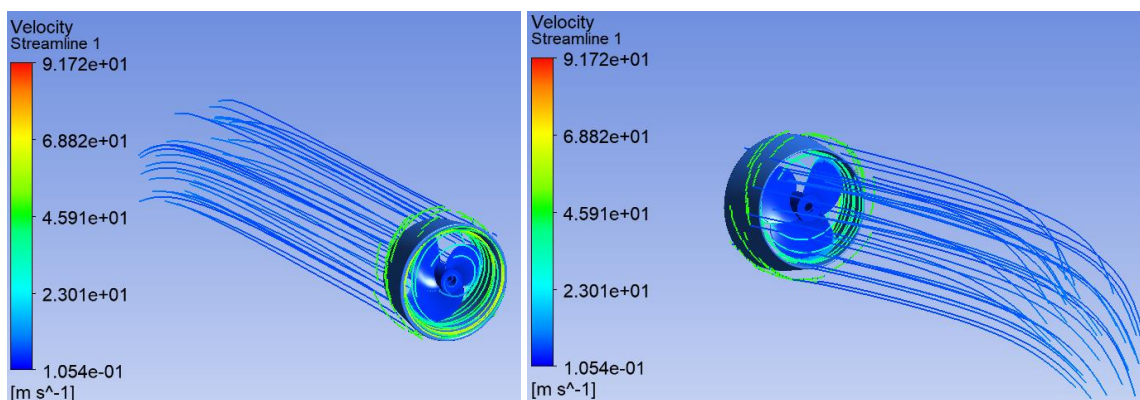


Figure 3.26: Velocity streamlines (ducted, $J=0.5$)

4 RESULTS AND DISCUSSIONS

4.1 Conventional Propeller

The open water characteristics of Wageningen-B series propeller are obtained using polynomial regression. The results are tabulated in the table below.

J	K_T	$10K_Q$	η_0
.0001	0.3370	0.4132	0.0001
0.1	0.3016	0.3776	0.1255
0.2	0.2628	0.3365	0.2454
0.3	0.2212	0.2912	0.3578
0.4	0.1773	0.2433	0.4578
0.5	0.1318	0.1941	0.5333
0.6	0.0852	0.1450	0.5541
0.7	0.0382	0.0974	0.4319
0.8	-0.0086	0.0527	-0.2053
0.9	-0.0547	0.0123	-6.2807
1	-0.0995	-0.0995	7.0022

Table 4.1: Open water data using regression analysis

Open water diagram is plotted based on the data in the **Table 4.1**.

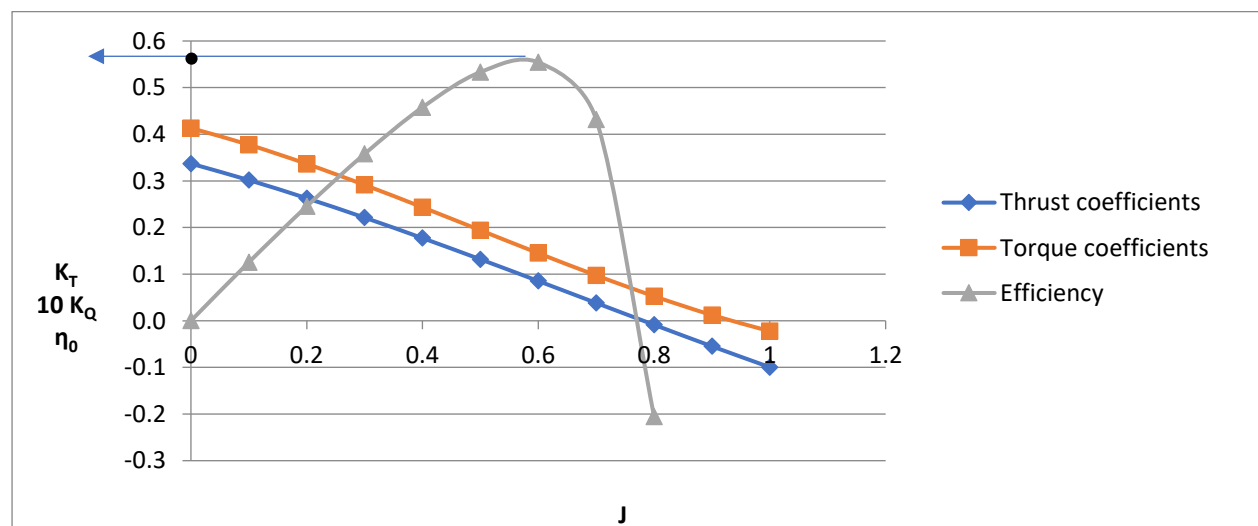


Figure 4.1: Open water diagram of conventional propeller using regression analysis

After $J = 0.7$, the value of thrusts become negative, and they are no longer useful. It provides a maximum efficiency of **56%** (approx.).

Numerical analysis has been performed on the same conventional propeller using ANSYS(Fluent) and open water characteristics are obtained as follows.

J	K_T	$10K_Q$	η_0
.0001	0.3038	0.3740	0.0001
0.1	0.2911	0.3456	0.1323
0.2	0.2641	0.3157	0.2628
0.3	0.2212	0.2714	0.3841
0.4	0.1759	0.2255	0.4899
0.5	0.1291	0.1785	0.5680
0.6	0.0817	0.1304	0.5906
0.7	0.0339	0.0806	0.4617
0.8	-0.0173	0.0261	-0.8311
0.9	-0.0775	-0.0387	2.8265
1	-0.1518	-0.1182	2.0173

Table 4.2: Open water data of numerical analysis using ANSYS

Open water diagram has been drawn based on the data of numerical analysis shown in the **Table 4.2**.

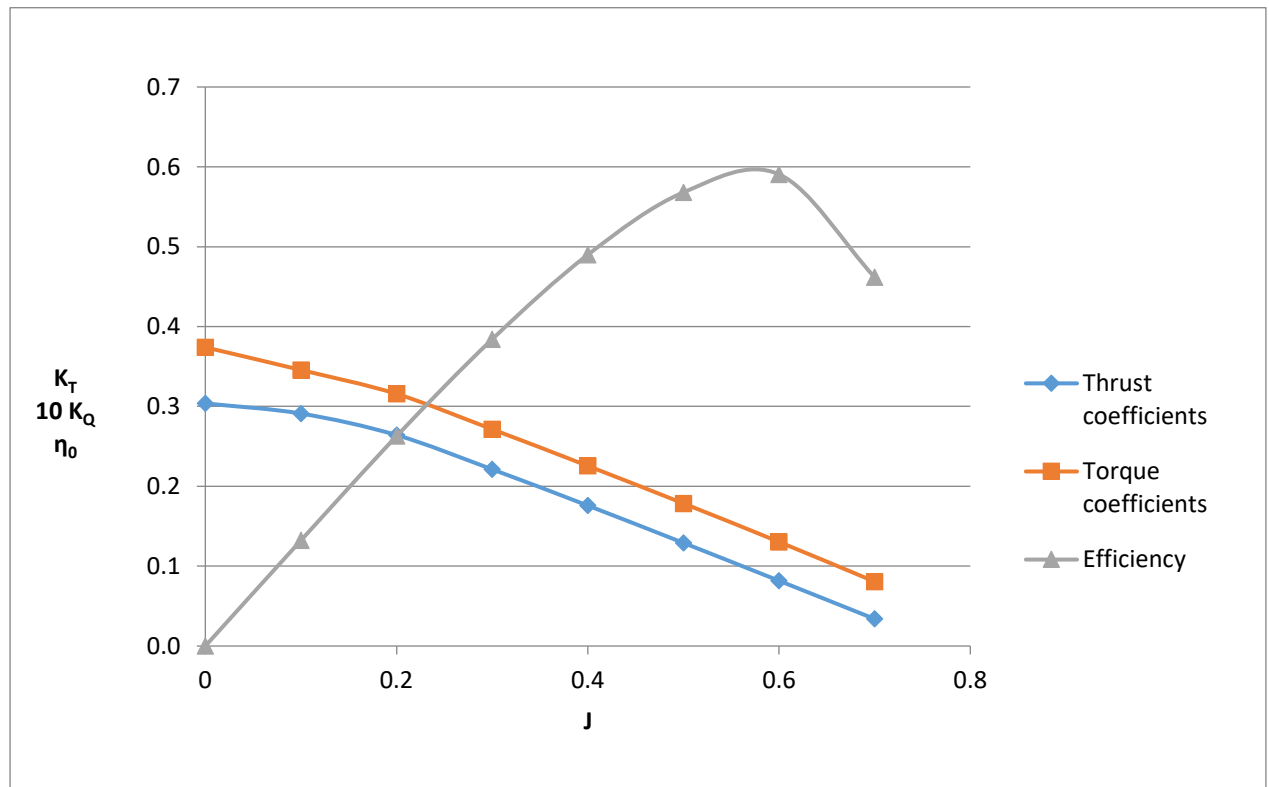


Figure 4.2: Open water diagram of numerical analysis

Numerical result also shows negative thrust after $J = 0.7$ and thus neglected. It provides a maximum efficiency of **60%** (approx.).

A comparison has been made between theoretical and numerical result in terms of percentage difference as shown in **Table 4.3**.

J	$\%K_T$	$\% 10K_Q$	$\%\eta_0$
.0001	9.8590	9.4799	0.4188
0.1	3.5041	8.4616	-5.4157
0.2	-0.4950	6.1777	-7.1121
0.3	-0.0224	6.8123	-7.3344
0.4	0.8051	7.3060	-7.0133
0.5	2.0277	8.0236	-6.5189
0.6	4.1578	10.0726	-6.5773
0.7	11.4879	17.1998	-6.8984
0.8	-100.6801	50.4272	-304.8188
0.9	-41.5465	414.5264	145.0031
1	-52.5393	-429.479	71.1907

Table 4.3: Percentage difference between Theoretical and Numerical Analysis

Here, our main concern is up to $J=0.6$ which indicates acceptable level of percentage of error. In some cases, the percentage errors are even lower than 1%.

A graphical representation of this comparison is shown using the data in **Table 4.1** and **Table 4.2**.

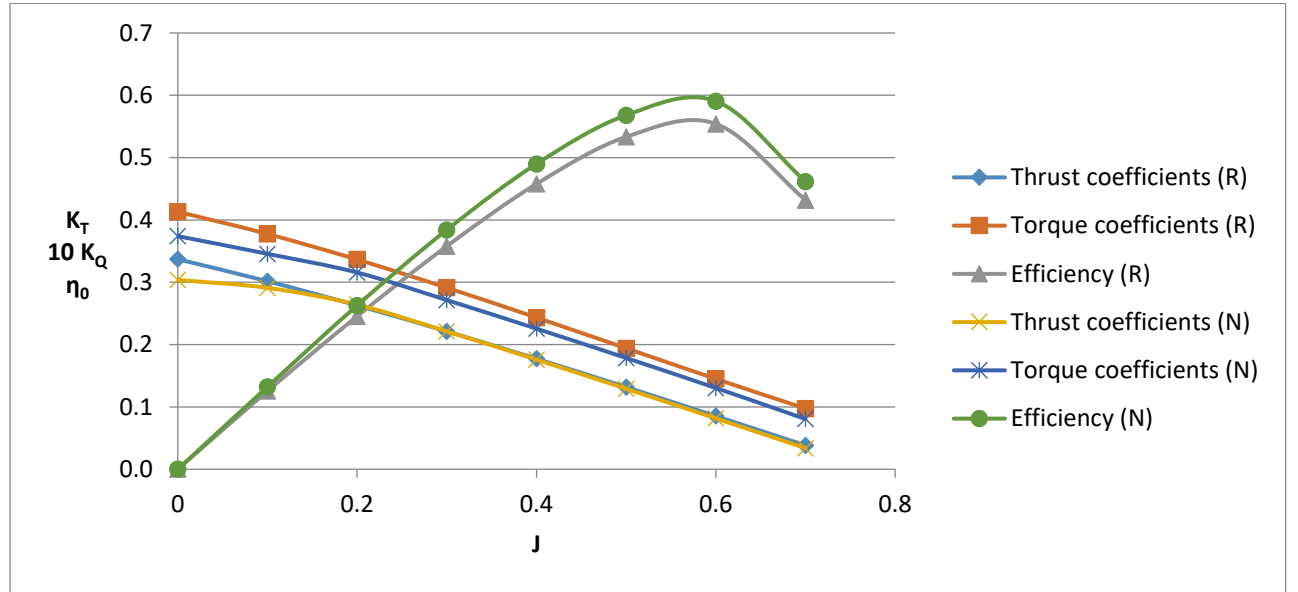


Figure 4.3: Open water diagram comparing Numerical Analysis with the Theoretical Value

From the above comparison, it can be concluded that the efficiency obtained from the numerical result is giving slightly higher values than the regression result. The percentage error in thrust is much lower than error in torque and efficiency.

Error percentage corresponding to the optimum value is shown in the table below.

J	0.3	.36	.4
$\% K_T$	0.02	.49	.81
$\% K_Q$	6.81	7.11	7.31
$\% \eta_0$	7.33	7.14	7.01

Table 4.4: Error percentage for optimum value

Further a comparison has been made with the results obtained by [Saha et al. \(2018\)](#).

J	% Error of results taken from paper		% Error of our results	
	K_T	$10 K_Q$	K_T	$10 K_Q$
0.1	13.36	17.24	3.50	8.46
0.2	15.15	19.23	-0.50	6.18
0.3	17.77	21.74	-0.02	6.81
0.4	23.27	25.00	0.81	7.31
0.5	32.77	31.25	2.03	8.02
0.6	57.89	50.00	4.16	10.07
0.7	163.33	75.00	11.49	17.20
0.8	-294.12	-158.82	-100.68	50.43

Table 4.5: Comparison with the mentioned paper

It shows that the percentage error in Thrust and Torque is comparatively lower than the results taken from the paper.

4.2 Ducted Propeller

A numerical analysis has been performed on the same conventional propeller with 19A duct mounted on it. The analysis gives the following result.

J	$K_{T,prop}$	$K_{T,duct}$	$10K_Q$	η_0
.0001	0.2135	0.0913	0.2425	0.0002
0.1	0.2045	0.0695	0.2307	0.1866
0.2	0.1847	0.0464	0.2086	0.3480
0.3	0.1584	0.0241	0.1798	0.4782
0.4	0.1284	0.0046	0.1473	0.5674
0.5	0.0919	-0.0125	0.1078	0.5788
0.6	0.0488	-0.0270	0.0609	0.3367
0.7	-0.0007	-0.0397	0.0065	-6.8804

Table 4.6: Open water data of the ducted propeller

The results shows that the thrust of the duct becomes negative from $J=0.5$ which means as the speed further increases, the performance of the duct decreases. The open water diagram for these results are shown below.

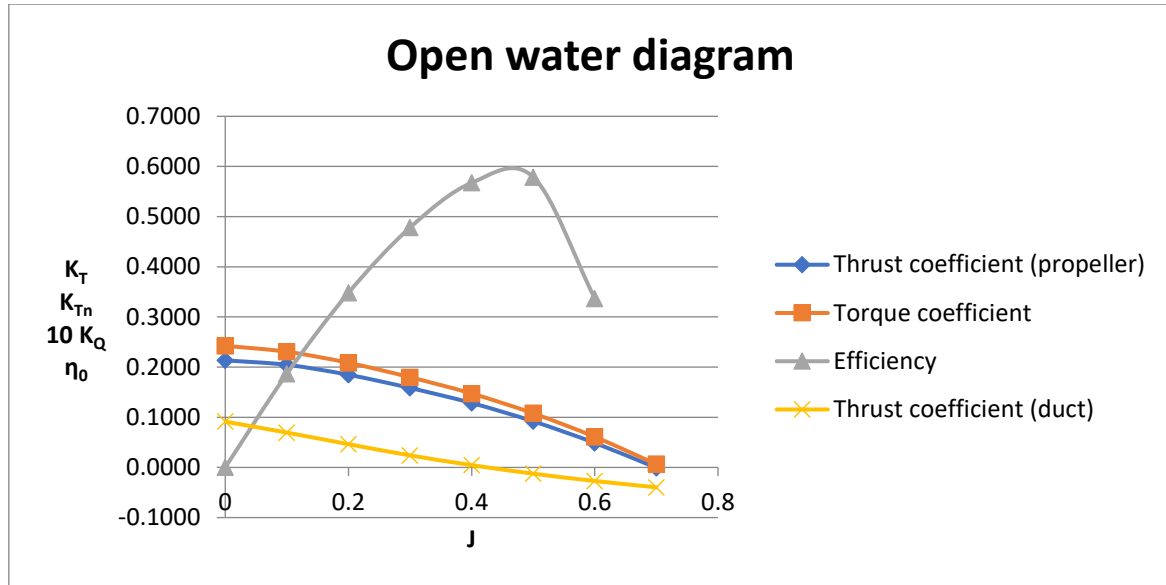


Figure 4.4: Open water diagram

The figure shows an optimum efficiency of near 60% and the thrust of the propeller is always higher than the thrust of the duct.

Furthermore, a comparison of efficiency has been made between the numerical results of the conventional propeller and the same propeller fitted with 19A duct as shown in **Figure 4.5**.

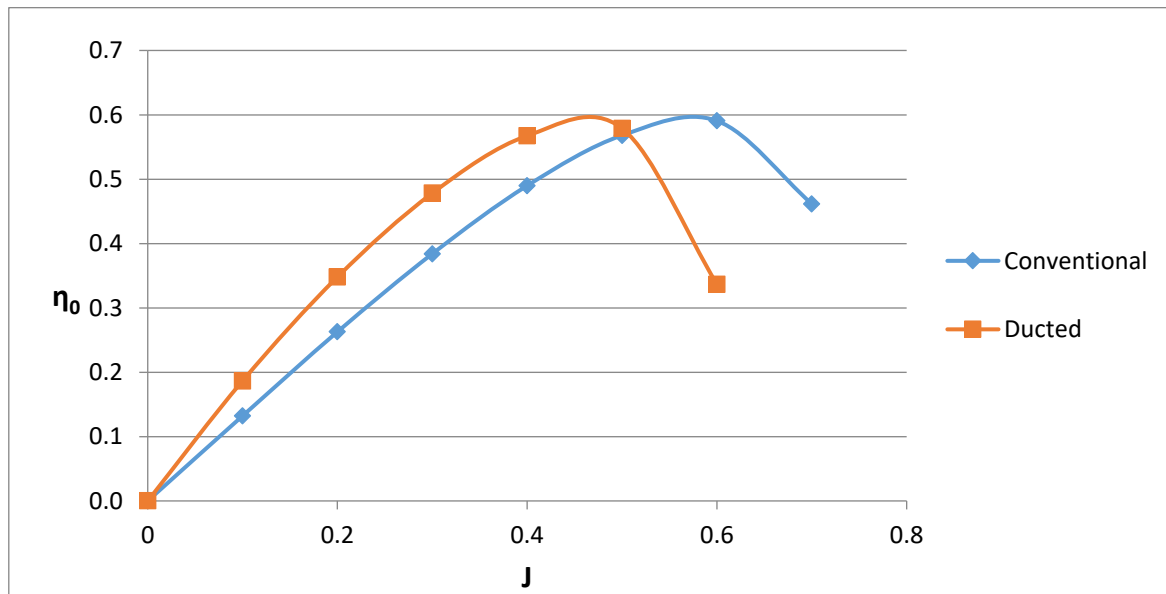


Figure 4.5: Comparison between conventional and ducted propeller

This comparison shows that efficiency of ducted propeller increases as the advance coefficient increases. Efficiency of ducted propeller is highest at $J = 0.48$ (approx.). Service speed corresponding to this advance coefficient is **13 knots**. For service speed higher than 13 knots, efficiency of the ducted propeller decreases significantly. Efficiency curves of ducted and conventional propeller intersect at $J = 0.5$. Service speed corresponding to this advance coefficient is **14 knots**. For service speed above 14 knots, conventional propeller provides higher efficiency than ducted propeller. Therefore, both conventional and ducted propeller can be useful depending on the service speed of a particular vessel.

5 CONCLUSIONS

Actual performance of a propeller can only be known after fully loaded service condition. In reality, there are numerous factors present that affect the performance of a propeller. For example, the effect of hull form, Engine propeller matching and fouling after certain period etc.

During design stage, towing test is performed to predict propeller performance. This test considers many possible conditions those may arise in service. Then the theoretical results are compared with the experimental results to predict the accuracy.

There is no model test result in case of this thesis. Instead CFD simulation has been performed via Ansys (Fluent). This is actually RANS solver, and the chosen method is $k - \epsilon$ realizable standard turbulent method. Then the regressional and numerical results have been compared to predict the accuracy.

Where there are no experimental results available due to the lack of a towing tank facility, this procedure can be very useful in predicting propeller performance.

6 REFERENCES

1. Bahatmaka, A., Kim, D. J., & Zhang, Y. (2018, August). Verification of cfd method for meshing analysis on the propeller performance with openfoam. In *2018 International Conference on Computing, Electronics & Communications Engineering (iCCECE)* (pp. 302-306). IEEE.
2. Barnitsas, M. M., Ray, D., & Kinley, P. (1981). *KT, KQ and efficiency curves for the Wageningen B-series propellers*. University of Michigan.
3. Boumediene, K., Belhenniche, S., Imine, O., & Bouzit, M. (2019). Computational hydrodynamic analysis of a highly skewed marine propeller. *Journal of Naval Architecture and Marine Engineering*, 16(1), 21-32.
4. Du, W., & Kinnas, S. A. (2019, June). Optimization Design and Analysis of Marine Ducted Propellers by RANS/Potential Flow Coupling Method. In *The 29th International Ocean and Polar Engineering Conference*. OnePetro.
5. DurgaNeeharika, P., & Babu, P. S. (2015, November). Design and analysis of ship propeller using FEA. In *Proceedings of International Conference on Recent Trends in Mechanical Engineering-2K15 (NECICRTME-2K15)* (Vol. 20, p. 21st).
6. Elghorab, M. A., Aly, A. A. E. A., Elwetedy, A. S., & Kotb, M. A. (2013). Open Water Performance Marine Propellers Using CFD. *Research Gate*.
7. Fitriadhy, A., Adam, N. A., Quah, C. J., Koto, J., & Mahmuddin, F. (2020). CFD prediction of b-series propeller performance in open water. *CFD Letters*, 12(2), 58-68.
8. Funeno, I. (2002). On Viscous Flow around Marine Propellers—Hub Vortex and Scale Effect—. *Journal of the Kansai Society of Naval Architects, Japan*, 2002(238), 238_17-238_27.\
9. Gaggero, S., Rizzo, C. M., Tani, G., & Viviani, M. (2012). EFD and CFD design and analysis of a propeller in decelerating duct. *International Journal of Rotating Machinery*, 2012.
10. Harish, B., Prasad, K. S., & Rao, G. U. M. (2015). Static Analysis of 4-Blade Marine Propeller. *Journal of Aerospace Engineering & Technology*, 5(2).
11. Kolakoti, A., Bhanuprakash, T. V. K., & Das, H. N. (2013). CFD analysis of controllable pitch propeller used in marine vehicle. *Global Journal of Engineering Design and Technology*, 2(5), 25-33.

12. Majdfar, S., Ghassemi, H., Forouzan, H., & Ashrafi, A. (2017). Hydrodynamic prediction of the ducted propeller by CFD solver. *Journal of Marine Science and Technology*, 25(3), 3.
13. Martínez-Calle, J. N., Balbona-Calvo, L., González-Pérez, J., & Blanco-Marigorta, E. (2002, January). An open water numerical model for a marine propeller: A comparison with experimental data. In *Fluids Engineering Division Summer Meeting* (Vol. 36169, pp. 807-813).
14. Mosaad, M. A., MM, H., & Yehia, W. (2011). Guidelines for numerical flow simulation around marine propeller. In *First International Symposium on Naval Architecture and Maritime, Istanbul*.
15. Motallebi-Nejad, M., Bakhtiari, M., Ghassemi, H., & Fadavie, M. (2017). Numerical analysis of ducted propeller and pumpjet propulsion system using periodic computational domain. *Journal of Marine Science and Technology*, 22(3), 559-573.
16. Parra, C. (2013). Numerical investigation of the hydrodynamic performances of marine propeller. *University of Galati, Gdynia, Master's thesis*.
17. Prakash, S., & Nath, D. R. (2012). A computational method for determination of open water performance of a marine propeller. *International Journal of Computer Applications*, 58(12).
18. Razaghian, A. H., & Ghassemi, H. (2016). Numerical analysis of the hydrodynamic characteristics of the accelerating and decelerating ducted propeller. *Zeszyty Naukowe Akademii Morskiej w Szczecinie*, (47 (119)), 42-53.
19. Saha, G. K., Maruf, M. H. I., & Hasan, M. R. (2018). Marine propeller design using CFD tools. *The Institution of Engineers, Bangladesh*, 64.
20. Shreyash C. Godge , Aditya M. Pandya , Shashank P. Shet , Dheeraj K. Amin, 2020, Performance Analysis and Enhancement of Marine Propeller, *international journal of engineering research & technology (IJERT)* Volume 09, Issue 02 (February 2020),
21. Szafran, K., Shcherbonos, O., & Ejmowski, D. (2014). Effects of duct shape on ducted propeller thrust performance. *Prace Instytutu Lotnictwa*.
22. TREJO, I., TERCEÑO, M., VALLE, J., IRANZO, A., & Domingo, J. E. R. Ó. N. I. M. O. (2007). Analysis of a ship propeller using cfd codes. *Calculation of the resistance and the wave profile of a, 3600*.
23. Triet, P. M., Thien, P. Q., & Hieu, N. K. (2018). CFD simulation for the Wageningen B-Series propeller characteristics in open-water condition using k-epsilon turbulence

model. *Science & Technology Development Journal-Engineering and Technology*, 1(1), 35-42.

24. Turunen, T., Siikonen, T., Lundberg, J., & Bensow, R. (2014). Open-water computations of a marine propeller using OpenFOAM. In *ECFD VI-6th European Congress on Computational Fluid Dynamics, Barcelona, Spain, 20-25 July 2014* (pp. 1123-1134).
25. Watanabe, T., Kawamura, T., Takekoshi, Y., Maeda, M., & Rhee, S. H. (2003, November). Simulation of steady and unsteady cavitation on a marine propeller using a RANS CFD code. In *Proceedings of The Fifth International Symposium on Cavitation (Cav.*
26. Yu, L., Greve, M., Druckenbrod, M., & Abdel-Maksoud, M. (2013). Numerical analysis of ducted propeller performance under open water test condition. *Journal of marine science and technology*, 18(3), 381-394.

APPENDIX

Appendix A: Resistance calculation by Holtrop and Mennen method

Holtrop and Mennen's method		
Parameters	Value	Unit
Waterline Length, L_{WL}	84.15	m
Length Between Perpendicular, L_{BP}	82.15	m
Breadth moulded, B	13.69	m
Draft moulded, T	4.28	m
Block Coefficient, C_b	0.79	
Ship Speed, V	10	knots
Prismatic Coefficient, C_p	0.817	
Midship Coefficient, C_m	0.967	
Density of water, ρ	1	tons/m ³
Volume of displacement, ∇	3,802.61	m ³
Displacement, Δ	3,802.61	tons
Water plane Co-efficient, C_{wp}	0.86	
Longitudinal Center of Buoyancy, L.C.B.	-1.23	m (aft,mid)
L.C.B as a % of L_{WL}	-1.46	% of L_{WL}
Transverse sectional area of BULB, A_{BT}	0	m ²
Immersed Transom area, A_T	0.89	m ²
Dynamic Viscosity, μ	.0008	m ² /s
Froude Number	0.181	

Parameter	Symbol	Formula	Values	Unit
1. Frictional resistance	R_F	$0.5 \rho V^2 S C_F$	33.596	KN
Frictional resist. coef.	C_F	$0.075 / (\log_{10} Re - 2)^2$	0.002	
Reynold's No.	Re	$\rho VL / \mu$	5.41E+08	
Form factor of the hull	$1+k_1$	$c_{13} \{ 0.93 + c_{12} (B/L_R)^{0.92497} (0.95-C_P)^{-0.521448} (1-C_P+0.0225lcb)^{0.6906} \}$	2.120	
Length of the run	L_R	$L (1 - C_P + 0.06 C_P lcb) / (4C_P - 1)$	4.551	
	T/L		0.051	

	C_{12}	$(T/L)^{0.2228446}$, if $T/L > 0.05$; $48.20 (T/L-0.02)^{2.078} + 0.479948$, if $0.02 < T/L < 0.05$; 0.479948 , if $T/L < 0.02$	0.515	
	C_{stern}	($C_{\text{stern}} = -10, 0$ or, $+10$ if the afterbody form is of V-shaped, Normal and U shaped sections respectively.	10.000	
	A_{BT}	transverse sectional area of bulb at the position where the still-water surface intersects the stem.	0.000	
	C_{13}	$1 + 0.003 C_{\text{stern}}$	1.030	
Wetted area of the hull	S	$L (2T+B) \sqrt{C_M(0.453 + 0.4425C_B -$ $0.2862 C_M - 0.003467 B/T + 0.3696$ $C_{WP}) + 2.38 A_{BT}/C_B}$	1534.986	m^2
2. Appendage Resistance	R_{APP}	$0.5 \rho V^2 S_{APP} (1+k_2)_{eq} C_F$	1.008	KN
	S_{APP}	2% of S	30.700	m^2
Appendage resist. factor	$1+k_2$	Rudder behind stern 1.3~1.5	1.500	
3. Wave Resistance	R_W	$c_1 c_2 c_5 \nabla \rho g \exp\{m_1 F_n^d + m_2 \cos(\lambda F_n^-$ $^2)\}$	9.142	KN
	F_n		0.179	
	T/B		0.313	
	L/B		6.147	
	L/T		19.661	
	C_P		0.817	
	L^3/∇		145.794	
	B/L		0.163	
	c_1	$2223105 c_7^{3.78613} (T/B)^{1.07961} (90-i_E)^{-$ $1.37656}$	2.567	
	c_7	$0.229577(B/L)^{0.33333}$, if $B/L < 0.11$; B/L , if $0.11 < B/L < 0.25$; $0.5-0.0625 L/B$, if $B/L > 0.25$	0.163	
	c_2	$\exp(-1.89\sqrt{c_3})$	1.000	
	c_5	$1-0.8 A_T/(BTC_M)$	0.987	
	λ	$1.446C_P-0.03 L/B$, if $L/B < 12$; $1.446C_P-0.36$, if $L/B > 12$	0.997	
	m_1	$0.0140407 L/T - 1.75254 \nabla^{1/3}/L -$ $4.79323B/L - c_{16}$	-1.982	
	c_{16}	$8.07981C_P-13.8673C_P^2+6.984388C_P^3$, if $C_P < 0.8$; $1.73014-0.7067C_P$, if $CP >$ 0.8	1.154	

	m_2	$c_{15} C_p^2 \exp(-0.1 F_n^{-2})$	-0.050	
	c_{15}	-1.69385 for $L^3/\nabla < 512$; 0 for $L^3/\nabla > 1727$; $-1.69385 + (L^3/\nabla - 8.0)/2.36$ if $512 < L^3/\nabla < 1727$	-1.694	
	d		-0.900	
Half angle of entrance	i_E		34	
	c_3	$0.56 A_{BT}^{1.5} / \{ B T (0.31 \sqrt{A_{BT}} + T_F - h_B) \}$	0.000	
4. Additional pressure resistance due to bulbous bow	R_B	$0.11 \exp(-3 P_B^{-2}) F_{ni}^3 A_{BT}^{1.5} \rho g / (1 + F_{ni}^2)$	0.000	KN
	h_B	where h_B is the position of the centre of the transverse area ABT above the keel line and T_F is the forward draught of the ship.	0.000	
	A_{BT}		0.000	m^2
	P_B	$0.56 \sqrt{A_{BT}} / (T_F - 1.5 h_B)$	0.000	
	F_{ni}	$V / \sqrt{\{ g (T_F - h_B - 0.25 \sqrt{A_{BT}}) + 0.15 V^2 \}}$	0.759	
5. Additional pressure resistance of immersed transom stern	R_{TR}	$.5 \rho V^2 A_T c_6$	0.000	KN
	A_T		0.890	m^2
	c_6	0.2 (1-0.2 F_{nT}), if $F_{nT} < 5$; 0, if $F_{nT} \geq 5$	0.000	
	F_{nT}	$V / \sqrt{\{ 2g A_T / (B + BC_{WP}) \}}$	12.085	
6. Model-ship correlation resistance	R_A	$0.5 \rho V^2 S C_A$	11.261	KN
	C_A	$0.006 (L+100)^{-0.16} - 0.00205 + 0.003 \sqrt{(L/7.5)} C_B^4 c_2 (0.04 - c_4)$	0.001	
	c_4	T_F/L , when $T_F/L \leq 0.04$; 0.04, when $T_F/L > 0.04$	0.040	
	T_F/L		0.052	
Total resistance	$R_T =$	$R_F(1 + k_l) + R_{APP} + R_w + R_B + R_{TR} + R_A$	92.637	KN

Appendix B: Taylor wake fraction

a ₀	-0.8715	b ₀	-0.1158	c ₀	1.716	V/C _B √L	0.771039
a ₁	2.49	b ₁	0.08859	c ₁	-2.378	V/□L	0.609121
a ₂	-1.475	b ₂	0.3133	c ₂	1.742	D _t	0.106778
a ₃	-0.3722	b ₃	0.2758	c ₃	-0.0308	δLCB	6.198983
a ₄	0.2525	b ₄	0.05432	c ₄	0.6931	D _w	0.348906
a ₅	0.226	b ₅	0.02419				
a ₆	-0.007176	b ₆	-0.4542				
		b ₇	0.6044				
		b ₈	0.05171				
		b ₉	-0.08622				

Thrust Deduction Coefficient, t	$t = b_0 + b_1 C_B + b_2 C_B^2 + b_3 (v/C_B \sqrt{L}) + b_4 (v/C_B \sqrt{L})^2 + b_5 (v/C_B \sqrt{L})^3 + b_6 (v/\sqrt{L}) + b_7 D_t + b_8 \delta LCB + b_9 C_B \delta LCB$	0.091 938
Taylor Wake Fraction, w _t	$w_t = a_0 + a_1 C_B + a_2 C_B^2 + a_3 (v/\sqrt{L}) C_B + a_4 (v/C_B \sqrt{L})^2 + a_5 D_w C_B + a_6 \delta LCB$	0.163 869
Relative Rotative Efficiency, η _R	$\eta_R = C_0 + C_1 C_B + C_2 C_B^2 + C_3 (v/\sqrt{L}) C_B + C_4 (D/V^{1/3})$	0.994 116
Hull Efficiency, □ _H	$\eta_H = (1-t)/(1- w_t)$	1.086 029

Appendix C: Thrust, Torque and Delivered power calculations

Thrust of the propeller,

$$T = \frac{R}{1-t}$$

$$V_A = V_S (1-\omega_t)$$

$$P_D = P_B \cdot \eta_{shaft} (1 - SM)$$

Thrust of the propeller,

$$T = \frac{R}{1-t}$$

Total resistance, R_T	92.63696	KN
	92636.96	N
Relative Rotative Efficiency, η_R	0.994116	
For machinery aft, the shaft transmission efficiency, η_s	0.98	
Density of water, ρ	1000	kg/m ³
Thrust of propeller, T	102016.1	N
Speed of advance, V_A	4.301057	m/s
Expanded blade area ratio, A_E/A_0 (Using Keller formula)	0.832457	
Delivered power, P_D (Considering 15% sea margin)	945.455	KW
Torque, Q	22.97305	KN-m

Appendix D: Propeller geometry

TABLE OF Y-face AND Y-back FOR DIFFERENT $\frac{r}{R}$ VALUES					
$\frac{r}{R} = 0.2$		$\frac{r}{R} = 0.3$		$\frac{r}{R} = 0.4$	
Y face	Y back	Y face	Y back	Y face	Y back
0.0210	0.0210	0.0151	0.0151	0.0084	0.0084
0.0195	0.0243	0.0134	0.0187	0.0069	0.0120
0.0178	0.0286	0.0118	0.0227	0.0055	0.0159
0.0146	0.0373	0.0088	0.0308	0.0036	0.0236
0.0117	0.0453	0.0062	0.0383	0.0023	0.0310
0.0090	0.0524	0.0041	0.0448	0.0012	0.0375
0.0065	0.0585	0.0025	0.0506	0.0007	0.0436
0.0044	0.0637	0.0013	0.0556	0.0003	0.0483
0.0013	0.0714	0.0002	0.0632	0.0000	0.0551
0.0000	0.0743	0.0000	0.0657	0.0000	0.0571
0.0004	0.0728	0.0002	0.0642	0.0000	0.0555
0.0023	0.0682	0.0010	0.0596	0.0002	0.0512
0.0039	0.0646	0.0020	0.0566	0.0005	0.0482
0.0060	0.0600	0.0033	0.0527	0.0011	0.0444
0.0088	0.0547	0.0052	0.0479	0.0020	0.0397
0.0125	0.0480	0.0078	0.0415	0.0036	0.0334
0.0149	0.0439	0.0095	0.0375	0.0048	0.0295
0.0175	0.0386	0.0116	0.0326	0.0062	0.0247
0.0210	0.0325	0.0144	0.0268	0.0084	0.0194
0.0264	0.0264	0.0192	0.0192	0.0125	0.0125
$\frac{r}{R} = 0.5$		$\frac{r}{R} = 0.6$		$\frac{r}{R} = 0.7$	
Y face	Y back	Y face	Y face	Y back	Y face
0.0025	0.0025	0	0.0025	0.0025	0
0.0020	0.0066	0	0.0020	0.0066	0
0.0016	0.0106	0	0.0016	0.0106	0
0.0009	0.0182	0	0.0009	0.0182	0
0.0005	0.0254	0	0.0005	0.0254	0
0.0002	0.0314	0	0.0002	0.0314	0
0.0001	0.0368	0	0.0001	0.0368	0
0	0.0410	0	0	0.0410	0
0	0.0467	0	0	0.0467	0
0	0.0485	0	0	0.0485	0
0	0.0471	0	0	0.0471	0
0	0.0431	0	0	0.0431	0
0.0000	0.0402	0	0.0000	0.0402	0
0.0002	0.0364	0	0.0002	0.0364	0
0.0004	0.0316	0	0.0004	0.0316	0
0.0010	0.0255	0.0000	0.0010	0.0255	0.0000
0.0016	0.0216	0.0001	0.0016	0.0216	0.0001
0.0024	0.0172	0.0003	0.0024	0.0172	0.0003

0.0038	0.0123	0.0007	0.0038	0.0123	0.0007
0.0062	0.0062	0.0015	0.0062	0.0062	0.0015
$\frac{r}{R} = 0.8$		$\frac{r}{R} = 0.9$		$\frac{r}{R} = 1.0$	
Y face	Y back	Y face	Y back	Y back	Y face
0	0	0	0	0	0
0	0.0022	0	0.0014	0	0.0005
0	0.0043	0	0.0027	0	0.0010
0	0.0082	0	0.0051	0	0.0020
0	0.0116	0	0.0072	0	0.0028
0	0.0145	0	0.0090	0	0.0035
0	0.0170	0	0.0106	0	0.0041
0	0.0191	0	0.0118	0	0.0046
0	0.0218	0	0.0135	0	0.0053
0	0.0227	0	0.0141	0	0.0055
0	0.0219	0	0.0135	0	0.0053
0	0.0193	0	0.0118	0	0.0046
0	0.0173	0	0.0106	0	0.0041
0	0.0148	0	0.0090	0	0.0035
0	0.0119	0	0.0072	0	0.0028
0	0.0085	0	0.0051	0	0.0020
0	0.0066	0	0.0039	0	0.0015
0	0.0046	0	0.0027	0	0.0010
0	0.0024	0	0.0014	0	0.0005
0	0	0	0	0	0

Appendix E: Duct geometry

Geometry data of the duct for nozzle the 19A the length-diameter ratio is, L/D	0.5
Diameter of the propeller, D (m)	1.83
Length of the duct, L (m)	0.915

x/L	y_{inner}/L	y_{outer}/L	x (m)	y_{inner} (m)	y_{outer} (m)
0	18.25		0	0.166988	0
1.25	14.66	20.72	0.011438	0.134139	0.189588
2.5	12.8	21.07	0.022875	0.11712	0.192791
5	10.07	20.8	0.04575	0.092141	0.19032
7.5	8		0.068625	0.0732	0
10	6.34		0.0915	0.058011	0
15	3.87		0.13725	0.035411	0
20	2.17		0.183	0.019856	0
25	1.1		0.22875	0.010065	0
30	0.48		0.2745	0.004392	0
40	0		0.366	0	0
50	0		0.4575	0	0
60	0		0.549	0	0
70	0.29		0.6405	0.002654	0
80	0.82		0.732	0.007503	0
90	1.45		0.8235	0.013268	0
95	1.86		0.86925	0.017019	0
100	2.36	6.36	0.915	0.021594	0.058194

Appendix F: Step by step Ansys setup for simulation

General

Mesh

Scale... Check Report Quality

Display...

Solver

Type

☒ Pressure-Based
☐ Density-Based

Velocity Formulation

☒ Absolute
☐ Relative

Time

☐ Steady
☒ Transient

☒ Gravity Units...

Gravitational Acceleration

X (m/s²) 0 P

Y (m/s²) -9.81 P

Z (m/s²) 0 P

Help

Models

Models

Multiphase - Off

Energy - Off

Viscous - Realizable k-e, Standard Wall Fn

Radiation - Off

Heat Exchanger - Off

Species - Off

Discrete Phase - Off

Solidification & Melting - Off

Acoustics - Off

Eulerian Wall Film - Off

Electric Potential - Off

Create/Edit Materials

×

Name

water-liquid

Material Type

fluid

Order Materials by

☒ Name
 ☐ Chemical Formula

Chemical Formula

h2o<I>

Fluent Fluid Materials

water-liquid (h2o<I>)

Fluent Database...

Mixture

none

User-Defined Database...

Properties

Density (kg/m3)

constant

Edit...

998.2

Viscosity (kg/m-s)

constant

Edit...

0.001003

Change/Create

Delete

Close

Help

Fluid

×

Zone Name

static_domain

Material Name

water-liquid

Edit...

☐ Frame Motion
 ☐ 3D Fan Zone
 ☐ Source Terms

☐ Mesh Motion
 ☐ Laminar Zone
 ☐ Fixed Values

☐ Porous Zone
 ☐ LES Zone

Reference Frame

Mesh Motion

Porous Zone

3D Fan Zone

Embedded LES

Reaction

Source Terms

Fixed Values

Multiphase

Rotation-Axis Origin

X (m)

0

constant

Y (m)

0

constant

Z (m)

0

constant

Rotation-Axis Direction

X

1

constant

Y

0

constant

Z

0

constant

OK

Cancel

Help

Fluid

Zone Name

rotary_domain

Material Name

water-liquid

Edit...

☒ Frame Motion
 ☐ 3D Fan Zone
 ☐ Source Terms

☐ Mesh Motion
 ☐ Laminar Zone
 ☐ Fixed Values

☐ Porous Zone
 ☐ LES Zone

Reference Frame

Mesh Motion

Porous Zone

3D Fan Zone

Embedded LES

Reaction

Source Terms

Fixed Values

Multiphase

Relative Specification

UDF

Relative To Cell Zone

absolute

Zone Motion Function

none

Rotation-Axis Origin

Rotation-Axis Direction

X (m)

0

constant

Y (m)

0

constant

Z (m)

0

constant

X

1

constant

Y

0

constant

Z

0

constant

Rotational Velocity

Translational Velocity

Speed (rpm)

393

constant

X (m/s)

0

constant

Y (m/s)

0

constant

Z (m/s)

0

constant

Copy To Mesh Motion

OK

Cancel

Help

- Boundary Conditions

contact_region-src (interface, id=11)

contact_region-trg (interface, id=12)

inlet (velocity-inlet, id=7)

interior-6 (interior, id=6)

interior-rotary_domain (interior, id=1)

interior-static_domain (interior, id=2)

outlet (pressure-outlet, id=8)

propeller (wall, id=10)

symmetry (symmetry, id=9)

wall-13 (wall, id=13)

wall-14 (wall, id=14)

Reference Values

Compute from

Reference Values

Area (m2)	<input type="text" value="1"/>
Density (kg/m3)	<input type="text" value="998.2"/>
Enthalpy (j/kg)	<input type="text" value="0"/>
Length (m)	<input type="text" value="1"/>
Pressure (pascal)	<input type="text" value="0"/>
Temperature (k)	<input type="text" value="288.16"/>
Velocity (m/s)	<input type="text" value="7.1904"/>
Viscosity (kg/m-s)	<input type="text" value="0.001003"/>
Ratio of Specific Heats	<input type="text" value="1.4"/>

Reference Zone

Solution Methods

Pressure-Velocity Coupling

Scheme

Spatial Discretization

Gradient	<input type="text" value="Least Squares Cell Based"/>
Pressure	<input type="text" value="Second Order"/>
Momentum	<input type="text" value="Second Order Upwind"/>
Turbulent Kinetic Energy	<input type="text" value="Second Order Upwind"/>
Turbulent Dissipation Rate	<input type="text" value="Second Order Upwind"/>

Transient Formulation

- ☐ Non-Iterative Time Advancement
- ☐ Frozen Flux Formulation
- ☐ Warped-Face Gradient Correction
- ☐ High Order Term Relaxation

Options...

Default

Solution Controls

Under-Relaxation Factors

Pressure
0.3

Density
1

Body Forces
1

Momentum
0.7

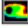
Turbulent Kinetic Energy
0.8

Turbulent Dissipation Rate
0.8

Turbulent Viscosity
1

Default

Equations... Limits... Advanced...

 **Force Report Definition** ✕

Name
thrust_force




Options

☐ Per Zone




Average Over(Time Steps)
1

Force Vector

X	Y	Z
1	0	0

Report Files [1/1]   




thrust_force-rfile

Report Plots [1/1]   

thrust_force-rplot

☐ Create Output Parameter ☐ Highlight Zones

OK Compute Cancel Help

Wall Zones   

propeller
wall-13
wall-14

Solution Initialization

Initialization Methods

- ☒ Hybrid Initialization
☐ Standard Initialization

More Settings...

Initialize

Patch...

Reset DPM Sources

Reset Statistics

Run Calculation

Check Case...

Preview Mesh Motion...

Time Stepping Method

Fixed

Settings...

Time Step Size (s)

0.03

P

Number of Time Steps

150

Options

☐ Extrapolate Variables

☐ Data Sampling for Time Statistics

Sampling Interval

1

Sampling Options...

Time Sampled (s) 0

☐ Solid Time Step

☐ User Specified

☒ Automatic

Max Iterations/Time Step

10

Reporting Interval

1

Profile Update Interval

1

Data File Quantities...

Acoustic Signals...

Acoustic Sources FFT...

Calculate

Help